SEARCH FOR OPTICALLY VISIBLE CLUSTERS ASSOCIATED WITH METHANOL MASERS

G. G. NYAMBUYA B.Sc.(Hons)

Dissertation submitted in partial fulfilment of the requirements for the degree Magister Scientiae in Physics at the Potchefstroomse Universiteit vir Christelike Hoër Onderwys

Supervisor: Prof. D. J. van der Walt D.Sc.

2002
POTCHEFSTROOM

"When I examine myself and my methods of thought, I come to the conclusion that the gift of fantasy has meant much more to me than my talent for absorbing positive knowledge ..."

Albert Einstein (1879 - 1955).

Abstract

We present a pilot study of the massive star formation region G264.29+1.47. A photometric and a two-point correlation function study of this region has been carried out in order to find out whether or not there is credit in focusing our attention on this region. From the two-point correlation function study, we report detection of two clusters in this region. The clustering in this region is found to be of the order of $\sim$ 56 arcsec. One of the clusters seems to be associated with the methanol maser while the other seems not. The photometric study carried out was an attempt to gain skills required for photometric analysis. Long and short exposure optical CCD images of this region were processed and the short exposure images were used in the final photometric analysis. A total of 28 stars in the short exposure UBV band were used for the photometric analysis. The colors-excess, visual extinction and approximate photometrically determined spectral types of the 24 stars were obtained. It is found that these stars are of spectral type earlier than A9.

Opsomming

Die resultate van 'n loodsondersoek op die galaktiese stervormingsgebied G264.29+1.47 word aangebied. Die doel van hierdie studie was om vas te stel tot watter mate navorsing op massiewe stervormingsgebiede met behulp van die fasiliteite van die Suid Afrikaanse Astronomie Observatorium te Sutherland, gedoen kan word. Om hierdie doel te bereik is optiese CCD waarnemings in 2001 van 'n aantal massiewe stervormingsgebiede gemaak en is G264.29+1.47 gekies vir verdere studie. Die eerste doelstelling was om vas te stel of 'n baie jong stertros wat met die stervormingsgebied geassosieer is, geïdentifiseer kan word. Met behulp van 'n twee-punt korrelasiefunksie is vasgestel dat daar wel tenminste een konsentrasie van sterre op die CCD beeld teenwoordig is. Die posisie van die stertros is met behulp van 'n autokorrelasiefunksie bepaal en dit stem ooreen met die posisie van die opties sigbare newel. Die autokorrelasiefunksie het ook die teenwoordigheid van 'n tweedestertros uitgewys. Dit wil voorkom asof hierdie tweede stertros ookmet die molekul\^erewolk geassosieer is en in ietwat ouer stertros is as die een wat met die omgewing van die maser geassosieer is. 'n Fotometriese studie in die U, B, en V bande is ook uitgevoer opsoveel as moontlik sterre in die waargenome veld. Die spektraaltipe van die sentrale ster is gskat as B2 terwyl Heydari-Malayeri(1988) dit as 'n O8.5V ster geklassifiseer het. Die resultate van hierdie studie het gewys dat verdere opvolgwerk beslisvrugbaar kan wees en dat dit ook na ander massiewe stervormingsgebied uitgebrei kan word. Die praktiese ervaring opgedoen in optiese CCD waarnemings en data analise was ook van groot waarde vir die toekoms.

Acknowledgements

I would like to thank the following people, institutions and organisations for making this study possible:

To my parents, my Mum and late Dad, many thanks for making me what I am today. You gave me the all I needed to acomplish my dreams.

To my Brothers and Sisters, especially George, many thanks for being there when I needed you.

To my Aunt, Mbuya Mabikwa, many thanks for standing by me at a time when I needed you.

To my friends Chris & Sue, Collin & Samia, Nina, Tilo, Emma, Rufaro, Pinkie, Cassandra, Kim, Andre, Sila, Edward, Daniel, Mlungisi, Owen, Lennox and last and certainly not least, Gibson, thank you for being my friends, for your friendship made me not feel lonely and hence enjoy my studies.

To my very special friend Rita, I say many thanks for being there when I needed you. Your friendship gave me the strength and courage I so much needed.

To Mathew Holleran, many thanks for helping me with the computer work and being a friend.

To Miss J. Bröwnn from going through this dissertation.

To the staff in the Physics department many thanks for your nice hospitality.

To Prof. H. Moral & Prof. C. Raubenheimer, I would like to say many thanks for admiting me to the Potchefstroom University School of Physics, only the Good Lord knows how grateful I am for what you did for me.

To Prof. Johan van der Walt, the man behind it all, many thanks for your patience, your guidance and everything, with you nothing would have been what it is today. Thank you so much for trusting and having confidence in me. You directed my worldline in the right path of my dreams. You certainly changed the stars.

To the National Research Foundation (NRF), thank you for the much needed financial support.

To the South African Astronomical Observatory, thank you for allowing us to use your facilities. I would like to extend my sincere thanks to the stuff for their warm hospitality especially the ladies in the kitchen for providing us with delious meals everyday during our stay.

Above all, I thank the Almighty God, Creator of Heaven and Earth, for making me who I am and giving me the opportunity to know part of his mind, that is, studying Physics, the esoteric subject of divine enquiry.

Contents

Chapter 1

Introduction

The study of young stellar clusters associated with regions of ongoing massive star formation can lead to the understanding of how massive stars are formed. The formation of massive stars is one of the most important unsolved problems of Astrophysics today. The study of massive stars is also essential to the understanding of the past, present and future evolution of our Galaxy because O and B stars have profound effects on their environment. They live short violent lives and manage in this short time to create sufficient excitement to keep astronomers busy behind their telescopes for many years, pondering trying to explain them. Powerful winds of massive stars impart momentum to the interstellar medium, thus they play an important role in determining the dynamics of the interstellar medium. The rate of star formation, composition and next generation of stars depends on the nature of the interstellar medium (Garmany, 1993).

At the end of their short lives, massive stars explode as supernovae, contributing heavy elements to the interstellar medium, creating shock waves which accelerate cosmic rays and possibly trigger the birth of the next generation of stars (Garmany, 1993). It is believed that in events such as supernovae, gravitational waves are emitted, that is, vibrations of space-time as predicted by Einstein's theory of General Relativity. If these waves are detected at all, they will open a whole new branch of physics and a new window into the Universe, that of Gravitational Wave Astronomy, thereby enhancing our knowledge of cosmogony, the evolution and the fate of the Universe.

1.1 Star formation

It can be stated with confidence that star formation is one of the most basic processes in the Universe. Without star formation the physical Universe as we know it would not have existed, and neither would life itself. Understanding star formation in all its different aspects is therefore of fundamental importance in modern Astrophysics. Since the dawn of mankind,

man has always pondered about the stars and strove to know them better. Progress in this seemingly metaphysical enquiry (how are stars formed?) dates back to the time of Laplace (Lada, 1999). Since then astronomers have postulated numerous scenarios about the formation of stars but to the present day this problem has somehow eluded man's imagination and no real solution compatible with all observations made to date has emerged (Churchwell, 1999). This is especially true for massive stars. Our present state of knowledge only gives us a blurred view of the grand picture of star formation. However, progress has recently been made to unveil the secrets of star-birth. The story of how stars are formed has been developed from both observation and theory.

The process of star formation begins with the gravitational collapse of a dense interstellar cloud of gas (molecular cloud), the interior of which is a dynamic environment subject to gravitational and radiative effects of nearby stars. Molecular clouds (MCs) are the densest and coldest parts of the interstellar medium. Approximately 50% of the mass of the interstellar medium is found in molecular clouds (Cabrit, 1992); as a result MCs play a very important role in the evolution of a galaxy. The gravitational collapse of a MC may begin spontaneously if a random fluctuation due to cloud turbulence causes the density in some regions of the cloud to be high enough for gravity to overcome the cloud pressure. The collapse may also be triggered by compression caused by an outside force, such as a shock wave from a nearby supernova event. For collapse to occur, the gravitational system must be unstable and for it to be unstable the mass (M_c) of the system (MC in this case) must exceed a certain mass known as the Jeans mass (M_j)[1] , that is

$$M_c > M_j \tag{1.1}$$

where

$$M_j \simeq \left(\frac{5k_BT}{G\mu m_H}\right)^{\frac{3}{2}} \left(\frac{3}{4\pi\rho_0}\right)^{\frac{1}{2}} \tag{1.2}$$

where k_B is the Boltzmann's constant, T is the initial temperature of the cloud, ρ_0 is the initial density of the cloud, μ is the mean molecular weight of the molecules found in the cloud and m_H the molecular mass of hydrogen. In this state the cloud undergoes free-fall. The free-fall time scale t_{ff} of this phase is given by,

$$t_{ff} = \left(\frac{3\pi}{32G\rho_0}\right)^{1/2} \tag{1.3}$$

where G is Newton's universal gravitational constant.

[1]In order to derive this condition one must make the following simplifing assumptions: (1) the MC (or gravitational system) is spherically symmetric, (2) the effects of Galactic rotation on the system are negligible, (3) the effect of Galactic magnetic fields on the system are negligible. This gives us insight into the development of protostars.

Once the collapse begins, it proceeds much more quickly in the central part of the cloud than in the outer regions because the free-fall speed of the cloud is proportional to the inverse of the distance (r) from the center of the cloud, that is $\propto r^{-1/2}$ (Bradley & Dale, 1996). As a consequence, a dense rotating central core forms. The lost gravitational potential energy is radiated freely through the optically thin envelope so that the collapse is isothermal. At first the core stays cold because infrared emission carries away all the heat energy gained by the gravitational compression. Once the core surpasses a certain density, the infrared radiation is trapped and the core heats up while the contraction slows. At this stage the budding star's major problem is its angular momentum. As it contracts, the conservation of angular momentum makes the core spin faster and if left alone it could eventually tear itself apart. To form a star, the contracting core must get rid of some of its angular momentum.

The behaviour of the cloud in which the star forms depends on the balance of forces within the cloud. As gravity contracts the core, increasing gas pressure due to an increase in temperature, pushes in the other direction. A few ions within the core grab the galaxy's local magnetic field that threads the core. As the core contracts, the field lines squeeze together and provide another outward pressure, slowing the contraction. If the core is dense enough, gravity ultimately wins the battle of the forces. As the core continues to contract, the magnetic field drags the ions to the outside, the inside becomes less charged, the magnetic field loosens its grip, and the core contracts ever faster, entering into a second phase of contraction (Kaler, 1997).

The second rapid collapse phase occurs when the temperature is high enough so that molecular hydrogen dissociates. This means heat is no longer trapped and collapse continues. At this stage, a star-like, optically thick hydrostatic core is formed inside the free-falling envelope. The collapse of the core is halted when the core becomes optically thick and cannot cool efficiently. The resulting increase in temperature causes an increase in the pressure which temporarily halts the collapse of the core.

The core now begins to grow in mass by accretion from the free-falling protostar envelope. The core slowly accretes more material and contracts towards the temperatures and densities characteristic of main-sequence stars on a Kelvin-Helmholtz time-scale given by

$$t_{KH} = \frac{GM^2}{RL} \tag{1.4}$$

where M, R and L are the mass, radius and the surface luminosity of the core respectively. The Kelvin-Helmholtz time scale t_{KH} is the time scale for the core's evolution in the pre-hydrogen burning phase (Lada, 1991).

When the core becomes so dense that gas pressure nearly counteracts gravity it enters once again into a phase of very slow contraction and heating and a protostar, as it is called, is formed. This protostar finally reaches hydrostatic equilibrium. This is a situation where

the inward gravitational pressure of the star balances the radiation pressure due to nuclear reactions in the star. When the core becomes hot enough for nuclear reactions to begin and hydrostatic equilibrum is achieved, the protostar becomes a true star . Accretion is halted when the radiation pressure and winds from the star prevent any more matter from falling in. This may proceed for some time well into the main-sequence phase of the star. In the case of a star of one solar mass, the temperature stabilizes at about 10^7 K. At this temperature, the main fusion reaction taking place is the proton-proton chain (hydrogen burning).

1.2 Massive stars

The above description of star formation is typical of low mass stars ($< 10\,M_\odot$). As the star accretes more matter, its radiation pressure increases until it reaches a stage where this process is halted because the radiation pressure has become so powerful that it blows off all the cocoon envelope material around it. This occurs at about $10\,M_\odot$ (Lada, 1999).

Massive stars are found deeply embedded in their stellar womb (the cores of giant molecular clouds) in their earliest stages of evolution. They form quickly and alter their environments and the yet unknown conditions under which they form (Walsh *et al.*, 2001). This makes it difficult to observe and study them directly at optical wavelengths. It is, however, possible to study them indirectly by studying their effects on the surrounding dust and gas. While embedded in the natal molecular cloud, they ionize the surrounding gas through their flux of ionising photons, giving rise to Ultra Compact (UC) HII regions. The photon flux will be absorbed by the surrounding dust and re-radiated at infrared wavelengths. UC HII regions are manifestations of newly formed massive stars that are still embedded in their natal molecular clouds.

The powerful winds of massive stars can also set up shock waves which affect the dynamics of the gas cloud and may cause it to collapse, thus paving the way for the next star births (Garmany, 1993). Their interaction with the surroundings can produce conditions favorable for masers to form which then serve as tracers of such star forming regions.

Over the last number of years a significant number of new massive star formation regions have been identified through their associated 6.7 GHz methanol maser emission. It seems that the main thrust at present in research on these sources is towards understanding what the observed linear alignment of the maser spots in many of these sources means. Some researchers interpret these observations as evidence for accretion disks around massive stars which obviously has important consequences for the understanding of how massive stars form (Goedhart, Van der Walt & Gaylard, 2000 and references therein). For example, if disk accretion really is a possibility, the disks would have to be (1) thin enough to survive the radiation field and (2) extend far enough to be replenished without the in-fall being affected by the radiation pressure

(Lada, 1999). It is not really clear how these massive stars manage to acquire so much matter. All we know is that they exist.

1.3 Young stellar clusters

A star cluster is a grouping of a few to many thousands of stars that are gravitationally bound to each other and therefore orbit a common center of mass. There are generally two types of star clusters, viz open clusters and globular clusters. Clusters of stars provide useful opportunities to observe the effects of evolution of stars in different stages of their lives and to test our existing models of star formation.

An open cluster, also known as a galactic cluster, is a loose conglomeration of up to hundreds of stars generally found in the plane of the disk of our Galaxy. A globular cluster is an enormous spherical ball of stars containing hundreds of thousands of members, typically found above or below the plane of our Galaxy's disk, in the region called the Galactic halo (Seab, 1995). Open clusters typically contain young stars while globular clusters typically contain more evolved stars. Because open clusters contain young stars they hold some of the secrets of star-birth.

Observations indicate that stars most frequently form in clustered environments - in rich clusters of many hundreds to many thousands of stars, or in smaller groups and aggregates containing of order of ten to a few tens of stars (Hillenbrand *et al.*, 1993). Understanding the properties of young stellar clusters is therefore important in so far as it appears to be a fundamental unit of star formation. It is only recently that their characteristics have begun to be understood (Brown *et al.*, 1991). In many clusters of stars the most massive members are generally found at the center of the cluster. This is particulary true for massive stars. They are unlikely to have formed elsewhere and evolved to the center by the time we observe them (Bonnell & Davies, 1998). This may mean that the formation of massive stars is linked to their environment. Cluster studies are therefore important from the viewpoint of star formation as is evident from recent publications which are discussed in the following paragraphs.

Recent work by Hillenbrand *et al.* (1993) and Belikov *et al.* (2000) on the very young cluster **NGC6611** has shown that there are numerous very high mass stars in that cluster with the most massive star having a mass of $80\,M_{\odot}$. These authors found 44 stars of spectral type earlier than B1.5 in the cluster. Taking these results of **NGC6611** into account one may ask whether massive star formation regions as identified through the presence of methanol maser emission have also formed so many massive stars.

Pandey *et al.* (2001) have carried out a detailed study of the open cluster **NGC 7654** using the 1.05-m Schmidt telescope of the Kiso Observatory. They obtained photometry for 17860 stars down to $V \sim 20$. Their studies have amongst other things raised some interesting questions about star formation. They found that star formation in this cluster was biased

towards relatively massive stars during the early phase of star formation whereas more low mass stars were formed in the last phase. They have also found that at the centre of this cluster there is no material and they attribute this to a possible supernova that might have occured in the past. One may then ask, why has star formation been biased towards relatively massive stars in the early phase of star formation in this cluster? If a supernova occured in the past, how did it affect the dynamics of the cluster? These are some of the interesting questions that have emerged from this study.

Using very deep I-band imaging obtained from the 1.55-m Strand Astrometric Telescope at the US Naval Observatory Flagstaff Station, of up to $I \sim 26.5$, Vrba *et al.* (2000) have discovered an embedded cluster of high mass stars in the soft gamma-ray repeater **SGR 1900 +14** region. This cluster, the authors claim, was previously hidden in the glare of a pair of $M5$ supergiant stars around this region. They managed to remove these stars by a point spread function subtraction. They suggested that young neutron stars, which are thought to be responsible for the **SGR** phenomenon, have their origins in proximate compact clusters of massive stars.

Herbig (1998) has conducted an extensive study of the very young cluster **IC448**. He obtained $BVRI$ photometry of about 260 stars in this cluster and spectroscopy of 80 of these stars. The photometry was carried out using a 2.2-m telescope. Herbig found that this cluster has little interstellar material remaining in the center. This may suggest that the massive stars that formed in this cluster have already eroded the interstellar material by supernova explosion.

The study of very young clusters associated with molecular clouds also allows for the estimation of the rate at which molecular clouds are being eroded by the very stars they gave birth to. Since the cluster is extremely young and has not been dispersed too much it is possible to estimate the initial distribution of gas (molecular cloud) with reasonable accuracy. Such information should be relevant in interpreting the mass spectrum of molecular clouds since the present observed distribution of masses of molecular clouds is due to cloud erosion, and is not necessarily the same as the distribution at the formation of the molecular clouds. Although this idea is not new, an estimate of the erosion rates for a number of clouds is nevertheless a worthwhile result. Different models for cloud erosion and dispersion were proposed in the past (see eg. Whitworth, 1979; Mazurek, 1980; Elmegreen, 1987) and might be tested if new data of the clusters we intend to study is obtained.

The studies cited above imply that young clusters associated with massive star formation are important from the viewpoint of massive star formation. The dynamic effects of massive stars on their environment can be used to find possible answers to some of the outstanding questions pertaining to massive star formation. For example, how do these massive stars manage to acquire so much mass in so short a period of time? If they do so by accretion, then, how does this accretion manage to overcome the powerful radiation winds of the already formed star? Could it be that electromagnetic forces also play an important role in the accretion process?

By studying the dynamics of such clusters it is possible to answer such questions and hence it is possible to understand how massive stars are formed.

1.4 Methanol masers

UC HII regions are one of the most prominent tracers of young high mass star formation regions. Their radio continuum emission is detectable at large distances in the Galaxy and various surveys have been conducted in the past to locate them. Methanol masers have also been detected in regions of high-mass stars and (mounting) evidence exists that these masers are tracers of high-mass star forming regions (Walsh *et al.*, 2000). The 6.7 GHz methanol maser emission is one of the strongest astrophysical masers in our Galaxy (Lee *et al.*, 2000). Extensive surveys have been carried out to detect class II methanol masers at 6.7 GHz and 12.2 GHz, water masers, hydroxyl masers and UC HII regions in our Galaxy (Goedhart, Van der Walt & Gaylard, 2000).

The fact that methanol masers (hydroxyl masers and water masers) are found near sites of massive star formation, makes these masers signatures, or tracers of high mass star forming regions. This fact alone is important for this study as it has been used as a selection criterion for the regions surveyed. At present, conditions giving rise to methanol masers are not well understood. Hypotheses have been put forward suggesting that the masers occur in circumstellar disks. However, there is a significant number of masers which do not appear to conform to these theories. It is possible that methanol masers are found in outflows, bow shocks or other areas in the star forming regions (Goedhart, van der Walt & Gaylard, 2000 and references therein; Lee *et al.*, 2000). Inspite of these uncertainies, methanol masers appear to be reliable indicators of high mass star formation and could be used for that purpose.

1.5 Motivation for this study

The basic motivation for this study is that it should act as a pilot study to see to what extent research on high mass star formation can be conducted using the existing facilities of the South African Astronomical Observatory (SAAO). Since these facilities consist mainly of optical telescopes it was necessary to find some aspect of high mass star formation that can be studied in the optical. Obviously this is not ideal. In addition, to investigate to what extent existing SAAO facilities can be used, there is also the need to find viable projects that can be continued using the South African Large Telescope which will become operational in a couple of years.

Most of the interesting things that happen during star formation occur inside molecular clouds which are not accessible for optical observations. One is therefore forced to be content with

studying the somewhat later phases of star formation when one is restricted to optical observations.

It has already been pointed out that most stars appear to form in clusters. From the stand point of observations it appears then quite logical that as a first step one would like to see if it is at all possible to find evidence of a cluster of stars that has recently emerged from a molecular cloud. It is interesting to note that clusters are studied either when they have fully emerged from the cloud or in the infrared when they are still embedded in the cloud. However, identifying very young optically visible clusters associated with regions of ongoing massive star formation will allow us to study the population of young stars emerging from the cloud. Optical photometry and spectroscopy still remains the most reliable way of determining the spectral types of stars and can be used to more accurately quantify the properties of the young stellar population.

The aim of this study is therefore a first step to explore this avenue of research which is new to the Space Research Unit of Potchefstroom University.

1.6 Thesis outline

This dissertation is subdivided into five chapters. The second chapter deals with the observations and data reductions. In this chapter, the data acquisation process is discussed and how the images obtained were cleaned. In the third chapter, the two-point correlation study of the field of G264.29+147 is presented. The two-point correlation function is discussed and then applied to this field thereby showing that there are two clusters in this field. In chapter four, a photometric study of the same field is presented. A total of 27 stars are analysed and plotted on color-color diagrams. Twenty four of these stars are dereddened and this enables us to determine possible approximate spectral types and extinctions for these stars is derived. Using the visual extinctions for these stars, an extinction map of G264.29+1.47 is plotted. In chapter five, the findings of the present study are presented.

Chapter 2

Observations and data reductions

2.1 Introduction

The basic point of departure in this dissertation is that methanol masers are indicative of very young high mass stars. This opens up other opportunities for research on star formation regions and these avenues must be explored. The primary aim of the present observations has been to search for very young optically visible clusters of stars associated with regions of ongoing massive star formation and to possibly study some aspects of these clusters. This programme has been initially envisaged to start with the present observations, that is, optical and infrared observations, and to be followed up later by spectroscopic observations on the cluster members (stated more precisely possible cluster members) in order to determine the spectral types of as many as possible of the cluster members and thus also to determine the distance modulus of the sources.

2.2 Source selection

In selecting a field to study, one cannot blindly select it from the methanol maser catalogue. For one they (methanol masers) are bright and can be seen over very large distances in the Galaxy. Blindly selecting a star formation region as identified by the presence of methanol masers may result in one ending up with a region so far away that optical imaging becomes difficult due to interstellar extinction. It is therefore important to take some care in selecting star formation regions which will be suitable for optical investigations. A first step in the selection process is therefore to obtain an estimate of the distance to the candidate star formation regions. For this, the kinematic distance has been found using the CS radial velocities (if available) from the observations of Bronfman *et al* (1996) and the rotation curve of Wouterloot & Brand (1989). The calculation itself was made using a computer code authored by Dr. M. J. Gaylard

Table 2.1: **List of observed fields**

Name	RA	Dec	Velocity (km / s)	Distance (kpc)
G254.66 +0.21	08 20 47.0	-36 12 34.0	-	-
G259.94 -0.04	08 35 31.7	-40 38 28.2	-2.0	< 1.0
G291.27 -0.71	08 48 49.4	-42 54 13.7	-23.4	$\sim 3.0 - 3.2$
G264.29 +1.47	08 56 27.8	-43 05 46.0	5.5	~ 1.3
G263.25 +0.52	11 11 53.0	-61 18 37.0	12.0	~ 2.2
G213.88 -11.84	11 11 51.2	-61 18 23.3	-	-

of the Hartebeesthoek Radio Astronomy Observatory. Since there are two solutions for the kinematic distance for objects inside the solar circle and since there are not clear indication which of the two are the correct, it was decided to select souces for which only one solution exists.

The sources selected using the aforementioned criteron were further inspected using images from the Digital Sky Survey (DSS). It is the aim of this search to find optically visible clusters, hence masers sources located in crowded star fields were rejected. The final observed sources are listed in table 2.1. For these fields, nebulosity associated with the masers sources could be seen on the DDS images which suggested a low value of interstellar extinction to these sources.

2.3 The Dandicam at SAAO

The discussion of the Dandicam at SAAO has been obtained from the SAAO webpage (http://www.saao.ac.za/facilities/dandicam/Dandi/Dandicam.htm). The 1.0 m telescope (also known as Elizabeth telescope) at SAAO was built by Grubb Parsons in 1964 and was originally erected in Cape Town. The Dandicam was installed on the 1.0 m telescope for the first time on 21 March 2000. The Dandicam, like its twin sister, the Andicam, is an imaging instrument capable of simultaneously recording at optical and infrared wavelengths. The two cameras were designed and built at Ohio State University. The primary purpose of the instrument is to search for micro-lensing events, follow-up to look for planets and anomalous behaviour of stellar objects.

The scientific goals of the instrument demand the highest possible photometric precision at a wide range of wavelengths. The Dandicam is capable of meeting the demands of projects that require a field of view large enough to include many comparison stars, to ensure accurate relative photometry even in marginal conditions. The quantum efficiency (see table 2.2) of the CCD of the Dandicam is excellent. The f-ratio of the the telescope of $f/10$ and the Dandicam optics have been matched to that.

Table 2.2: **Quantum efficiency of the CCD for different bands**

Band	U	B	V	R	I
QE (%)	~ 75	~ 85	~ 92	~ 90	~ 80

2.3.1 The CCD chip

The 1024 pixel × 1024 pixel CCD chip has a number of scattered blemishes that can be seen on a flat field image (visit http://www.saao.ac.za/facilities/dandicam/Dandi/Dandicam.htm to see an image of it). The chip is read by two amplifiers at opposite ends. These inevitably have different gains, and bias levels which account for the apparent difference between the top and the bottom halves. The filter occults the edges of the beam, resulting in an unvignetted field of 9.6 arcmin in diameter. There are 16 columns of overscan on each side of the readout. It is necessary to have a bias frame in order to get rid of the apparent difference between the top and bottom halves. The plate scale of the CCD chip is 0.28 arcsec/pixel .

2.3.2 The IR chip

The nominal size of the IR chip is 2048 pixel × 2048 pixel. Only one quadrant is guaranteed by the manufacturer (for a description of the cosmetic defects of the IR chip visit the website http://www.saao.ac.za/facilities/dandicam/Dandi/Dandicam.htm). The IR detectors are made of hybrid HgCdTe arrays. Each quadrant of the IR chip has a field of view of 1.7 arcmin × 1.7arcmin.

The IR observations made were not untilized because the IR chip has some cosmetic defects which make the data obtained from it somewhat unsuitable to work with. Follow-up of near infrared observations with the 1.4-m Japanese telescope at Sutherland are, however, being planned.

2.4 Observations

The observations were made during the period 27 February to 3 March 2001 by D. J. van der Walt and the author on the 1-m telescope of the SAAO at Sutherland. Both optical and infrared images of the sources listed in table 2.1 were obtained. Weather conditions were photometric on most of the nights. Flat field exposures were taken just after sunset. On most of the nights problems were experienced with the auto-guiding system which the technicians could not fix, and observations were continued without the auto-guiding system, hence exposure times were limited. A further uncertain factor at the time of observations was the avoidance of saturation of the stellar images on the CCD. This also prompted us to obtain shorter exposure images. The longer exposure images for the field of G264.29+1.47 were made on the

last night in an attempt to get deeper images. During the time of observation of the source G264.29+1.47 on the last night, it was in the southeast sky. This meant observations were limited due to clouds moving in from the north west. Conditions appeared to be photometric in the direction of the source, although later analysis of the data suggested that the conditions were not photometric.

Table 2.3 shows a summary of the observations made. Column 1 gives the name of the field that was observed. Column 2 gives the night on which these observations where made. Column 3 shows the band together with the integration time and number of images made. That is, 1×300 B would mean that 1 image in the B-band was made whose intergration time is 300 s. Column 4 gives the standard star observations made. Standard star observations where made before or after the observations of the field. The standard stars that we used were obtained from the E-region standard star catalogue of SAAO. Column 4 gives the weather conditions of the night of observation.

For this study, only the field of G264.29+147 was analysed. The observations of night 3 of this field were processed together with those of night 7 and the data derived from these observations will be refered to as the short exposure data set and the long exposure data set respectively. The short exposure data set has short integration times compared to the long exposure data set, hence the terminology short and long exposure data set respectively. The main reason for making the short exposures was to avoid saturation of the images.

A new set of optical and spectrocopic observations of the field of G264.29+1.47 were made in February 2002 by D. J. van der Walt at the SAAO. Unfortunately time constraints did not permit these observations to be part of this dissertation. Only a two-point correlation function study was made of these observations. This data set will be refered to as the 2002 data and that of 2001 will be refered to as the 2001 data.

2.5 Data reductions

Data reduction can be defined as the process or steps taken to obtain quality interpretable data from a given set of data not directly interpretable by the human mind. In the case of astronomical data reductions, this involves both cleaning of the data and the analysis of it. Cleaning is a step taken to minimize the influence of data acquisition imperfections on the estimation of the desired astronomical quality of the raw data. Analysis is the process of converting the data to a form interpretable (usually numerical) by the human mind.

Table 2.3: The Observations table

Field	Night	Integration time (s)	Standard Star Observations	Weather Condition
G254.66+0.21	1	1×300 B, 1×200 V, 1×100 R I	1 Before & 1 After	Good
G259.94-0.04	2	2×100 $UBVI$	1 After	Good
G291.27-0.71	2	2×100 UB, 4×5 V, 4×10 R, 4×20 I	1 Before & 2 After	Good
G264.29+1.47	3	2×100 UB, 5× 4 V, 4×10 R, 3×30 I	1 After	Good
G264.29+1.47	3	2×100 UB, 4×10 B,4×5 V,4×10 R,3×30 I	1 Before & 2 After	Good
G291.27-0.71	3	2×100 U, 4×10 B, 4×5 VRI,	2 After	Good
G263.25+0.52	4	1×50 UB, 1×10 V ,1× 5 RI	1 Before & 1 After	Not Good
G263.25+0.52	4	2×50 $BVRI$, 1×20 V	1 After	Not Good
G213.88-11.84	5	3×150 U, 2×100 I, 4×80 BR,4× 40 V ,	1 Before & 1 After	Good
G263.25+0.52	6	4×100 U, 4×160 VR,4×90 I, 6×35 B	-	Good
G291.27-0.71	6	2×100 U, 8×20 VR, 5×35 B,6× 30 I	2 Before & 2 After	Good
G264.29+1.47	7	4×200 B, 4× 200 VI, 4×100 R,	1 Before & 1 After	Not Good

2.5.1 IRAF software

For the data reductions, the Image Reduction and Analysis Facility (**IRAF**) software package was used. The **IRAF** software package is useful for general image processing and is designed specifically for the reduction of astronomical data. It is a product of and is distributed by the National Optical Astronomical Observatories (NOAO) of the United States of America.

IRAF software runs on a wide selection of UNIX-based systems. It provides the user with a wide range of image processing tools using a command line interface. Commands called tasks are executed to perform various functions. Each task has its own parameter file that the user can modify to affect the output of the task.

2.5.2 Why clean the data?

In order to understand the data reduction steps, it is necessary to first understand the factors affecting the image on the CCD. These factors will be explained in brief in this section. This discussion follows that of Gullixson (1992).

1. The raw CCD image obtained at the telescope is a combination of the photons of the object of interest and background photons altered by the spatial systematics present in the imaging system. We will follow the photons from the object of interest until they reach the CCD to form the raw CCD image in order to see how the object photons and background photons combine to form the raw image at the telescope.

2. Denote the object photons by *obj*. Between the object of interest and the telescope, the object photons are joined by background photons from the foreground, background

objects, zodiacal light, light from the atmospheric thermal emission, emission lines, scattered light from the moon and nearby city lights. Call these the *sky* photons.

3. As the *obj* photons and the *sky* photons enter the telescope structure they are joined by thermal photons emitted by the telescope structure. Denote these by *tbe*.

4. All these photons travel through the optical elements of the telescope and the imaging system. A fraction of the photons is lost to optical transmission variations (*otv*). As the remaining photons strike the CCD, a fraction, determined by the CCD quantum efficiency (QE), will be converted into electrons within the CCD. If the observations are taken in a narrow bandwidth or there are bright, narrow emission lines present in the atmosphere, interference fringes may be present. Denoted this by $fringe$.

5. During the exposure, dark emission from the CCD itself (denote it *dark*) will be accumulated along with the detected photons. There may in addition be charge present due to preflash ($flash$) before the start of the exposure. During the readout of the CCD, charge may be skimmed from columns having a deferred charge (*skim*) and a bias level (*bias*) is added to the signal.

6. From this we see that the raw CCD image (raw) can be written as

$$raw = (obj + sky(1 + fringe) + tbe)(otv)(QE) + dark + flash - skim + bias. \quad (2.1)$$

7. If it is assumed that optical transimission variations and fringing are negligible, then from equation (2.1) we can write

$$obj = \frac{raw - dark - flash + skim - bias}{QE} - sky. \quad (2.2)$$

8. All the terms on the right hand side of equation (2.2) can in principle be determined so we can convert or reduce the raw image to produce an image of the object of interest obj. This process is called the cleaning of the image.

9. In modern telescopes, CCDs work at $180K$. The CCD is housed in a cryostat containing liquid nitrogen at a temperature of $77K$ so that the effect of dark emission is minimized. Dark emission correction was not taken into account in the cleaning process since, for the aforementioned reasons, it does not affect the quality of our data. Hence it can be eliminated from equation (2.1) and hence equation (2.2).

Knowing the processes that affect the data, one must devise some means of "washing" away the "dirt". The cleaning steps will be discussed in the following subsections.

2.5.3 Overscan

It is common to take what is referred to as "overscan" data with the routine operation of a CCD. This is not really a source of noise in the classical sense, but failing to take the information derivable from the overscan into account can lead to serious problems. The overscan data is acquired by continuing to readout a line of the CCD past its real physical extent. In the physical picture of CCDs being readout by sequential shifting of buckets of electrons, overscanning amounts to analysing the zero offset on the empty unexposed buckets, that is, it provides a measure of the electronic bias level that physically indicates zero photons counted. To make use of the overscan information a user defined task **Doscan**[1] was applied under the IRAF environment to all the images before anything was done on them in order to take the information derivable from the overscan into account.

2.5.4 Bias correction

To correct for bias level one needs very good bias frames. To obtain a good bias frame one must average many such frames. For the present reductions there was only one bias frame. This bias frame was subtracted from all the raw images, obtaining new bias subtracted images (call them *image*). If the CCD is free from fringing and if there is no significant background contribution due to telescope background emission and dark emission and if we considered dark emission to be insignificant then we have,

$$image = (obj + sky(1 + fringe) + tbe)(otv)(QE). \tag{2.3}$$

2.5.5 Flat Fielding

Following the discussion of Gilliland (1992) flat fielding will be discussed here. Flat fielding is one of the most common and by far the most important reduction step. It is also one of the more difficult to obtain correct calibration data to support. Flat fielding corrects for pixel to pixel gain variations. Different pixels have different quantum efficiencies resulting from small structural variations on the CCD and this causes the gain variations from pixel to pixel even for perfect uniform illumination of the CCD.

In principle a calibration flat field is simple to obtain: one simply needs to expose the CCD to a uniform intensity illumination (hence the terminology flat field) and take a well exposed integration. Any resulting pixel to pixel variations directly reflect the QE differences of primary interest. In practice there are difficulties involved. These difficulties arise from two principle sources: (1) providing a uniform illumination to the CCD at the level of one part

[1]The computer code of this user defined task **Doscan** was provided by one of the members of staff at SAAO, that is John Menzies. It was then incorperated into the standard IRAF software package.

in a thousand (or better) that is sometimes desired, and (2) the QE variations often have a dependence on the wavelength, therefore the flat field is only valid if the light distribution over the filter bandpass is the same as for the objects being observed. The first is difficult to satisfy and the second is essentially impossible to satisfy for broad band photometry in general.

Substantial amount of time was taken to obtain the flat fields although it was later discovered that these flat fields were saturated. This discovery was by D. J. van der Walt (at the time of writing up this dissertation) during the 2002 observations at SAAO. The implication of the saturated flat fields is that additional artificial differences between the images of the stars on the frame can not be removed. Although an attempt was made towards obtaining photometry of the stars on the frame of G264.29 +1.47, the fact that the flat fields were saturated has to be kept in mind when evaluationg the results. If accurate photometry of this field is to be obtained, then there is need to re-observe these fields. As mentioned, this has already been done by D. J. van der Walt . It is hoped that these observations are better than the 2001 observations.

The twilight sky was used as a flat field source. This was done just after sunset when the sky was clear and void of stars. This method has the advantage that many photons are readily available allowing for a good signal to noise (S/N) ratio in the results. Flat fields belonging to the same band pass were combined (using the task **imcombine** found in the IRAF software) to give a median average flat-field. The mean flat field, which is the median average flat field ($\langle flat \rangle$) image can be written as

$$\langle flat \rangle = (otv)(QE) + bias. \tag{2.4}$$

The flat fields were bias subtracted to obtain the new bias subtracted flat field $\langle flat \rangle_{bias}$

$$\langle flat \rangle_{bias} = (otv)(QE). \tag{2.5}$$

Now if we divide equation (2.3) by equation (2.5) we get the object image obj that is

$$obj = \frac{(image - bias)}{(\langle flat \rangle - bias)}. \tag{2.6}$$

This is the equation which describes the basic cleaning steps. The image names were put into one file and also the bias and flat-fields. The task **ccdproc** was then executed to clean the images.

2.5.6 Combining of images

Having cleaned the CCD images, there are two major tasks that are left to be done. The first task is to combine as many as possible frames of the same region of the same band-pass to produce a final image. Combining the images has the advantage of increasing the S/N ratio. The second task is to remove image defects such as bad pixels due to non-linear or dead columns and transients such as radiation events.

The first step is to register the images. Registering is done so that the computer can recognise the same x-y points on the different CCD frames. The task **xregister** was used to register the images. Before registering is done, one must choose a reference image and a portion of that image common to all the other images so that this may be compared to all other images. Thereafter the images are registered.

The task **imcombine** was used to obtain the final images by taking the median average of the registered images belonging to the same band and combining them. The median rather than the mean average of the registered stack of images was taken because this reduces the residual effects of spatial systematic errors remaining in the individual images and eliminates the effects of non-linearity or bad pixels. An added benefit is that radiation events and other transients will also be eliminated from the final image.

It is unfortunate that the final cleaned and combined images could not be presented here. The reason being that no good quality images could be obtained from the 2001 data due to their relative short integration time but an image of the field of G264.29+1.47 from the 2002 observations will be shown later.

2.5.7 Photometric reductions

The steps leading to the photometric data will be discussed in this section. That is, the photometric data reductions steps that lead to obtaining the magnitudes and the color indices of the program stars.

1. First, the airmasses of the stars on the different images were computed using the task **setairmass** in the **astutil** package of **IRAF**. The task **setairmass** reads all the information it needs from the image headers. The airmass is the measure of the path length through the earth's atmosphere in the direction of the star being observed and is approximately given by sec(z) where z the angle between the zenith and the line joining the star and the Earth.

2. The next task that needs to be done is to locate the stars on CCD frame. This was done using the task **daofind** in the interactive mode. Interactive here simply means the

stars are picked up on the CCD frame using the computer mouse. They were picked in this way so that as many stars as is possible are picked up. This has the disadvantage of picking up saturated stars. However, this was checked at the end of the photometric reductions and found that most of the stars that were saturated were those found at the edge of the CCD. These stars are not important and hence do not affect the quality of the output data.

3. The instrumental magnitudes of the standard stars were obtained by running the task **phot** on the images of the standard stars. An aperture size (radius) of 14 pixels was used for the standard stars. The parameter files, **datapars, centerpars, fitskypars, photpars** were set to read the correct values. For each frame the standard star was identified interactively using the cursor and the task **phot** was run on the image to obtain the instrumental magnitudes. Using the task **txdump** all the names of the files containing the instrumental magnitudes of the stars were stored in one file. The task **txdump** extracts a field from a given file.

4. A standard star catalogue consisting of the magnitudes and color indices of the standard stars was created using the task **mkcatalog**. This catalogue file was used as a calibration file for the program stars.

5. With all the parameters set to read the right values, the task **phot** was run on the images to obtain their instrumental magnitudes. After this a point spread function (PSF) was generated around each star using the task **psf.** When running the task **psf,** one must try to select an uncrowded bright star. After doing this, the task **nstar** was run on the files generated by **psf.** The task **nstar** checks how good the psf is. If there were any neighbours around the psf-star, the psf radius was decreased, because this meant that the radius used in the previous run of **nstar** was too large. Next the task **substar** was run (using a smaller radius) and the subtracted frame displayed. The task **substar** subtracts a given star from the CCD frame. If the residuals of the psf stars looked consistent then all was considered fine, else the psf fitting process was started all over again. Next, any neighbouring stars around the psf star were removed by editing the psf stars and the task **substar** was re-run. The task **psf** was run on the subtracted file using the normal psf radius again. The task **nstar** was run on the original frame using the normal psf radius and the revised **psf.** Finally, the task **substar** was run and the results displayed. If the psf stars were nicely removed then all was considered fine, else the neighbours were removed around the psf star and the psf was re-computed.

6. The task **allstar** was run and the subtracted frame displayed to see if the stars were nicely removed. The task **allstar** computes the psf on all the stars whose photometry one desires. The task **daofind** was run on the subtracted frame and the task **phot** was run on the original frame with the co-ordinates generated from the previous run of the

Table 2.4: The extinction coefficients

U	B	V	R	I
0.54	0.27	0.15	0.10	0.07

task **daofind**. The two photometry files were then combined using the task **pappend**, and **allstar** was run on the combined file. After all this had been done, next was to determine the aperture corrections and transform the instrumental magnitudes into the standard system using the task **invertfit**. The task **invertfit** converts the instrumental magnitudes to the standard system of magnitudes.

To convert to the standard system of magnitudes one must solve a set of simultaneous equations. For the UBV system, the set of equations is

$$u = U + C_U + ColorTerm \times (U - B) + E_U \times Airmass \tag{2.7}$$

$$b = B + C_B + ColorTerm \times (B - V) + E_B \times Airmass \tag{2.8}$$

$$v = V + C_V + ColorTerm \times (B - V) + E_V \times Airmass \tag{2.9}$$

where u, b and v are the instrumental magnitudes, E_U, E_B, and E_V the extinction coefficients and C_U, C_B and C_V the zero-points. The extinction coefficients listed in table 2.4 were used for the present study. These were obtained from SAAO and the standard procedure at SAAO is to take the values as fixed and we have followed that convension. The airmass is known from the observations. The term containing the $ColorTerm$ was set equal to zero because it was considered negligible for the following reasons. The errors in the zero-points are of the order of 0.01 and this sets an upper limit to the number of decimal places in the final colors. The color term itself is or the order of 0.01. Typical values are ~ 0 for the V-band, -0.02 to 0.04 for the B-band and 0.00 to 0.04 for the U-band (), thus droping the term containing the $ColorTerm$[2] could not make much of a difference within the error magines.

The details of the observations of the standard stars is given in table 2.6 and the standard magnitudes and colors of these stars is given in table 2.5.

[2]The standard procedure in **IRAF** is to set the color term to zero.

Table 2.5: **The Visual magnitudes and colors of the standard stars.**

Star	V	$B-V$	$U-B$	$V-R$	$V-I$
E417	9.602	0.200	0.164	0.136	0.265
E4103	9.360	1.448	1.668	0.784	1.492
E519	9.820	0.478	0.053	0.279	0.556
E607	8.780	0.119	0.104	0.072	0.154
E394	8.630	1.5383	1.930	0.858	1.691
E424	8.505	0.489	-0.017	0.282	0.568

2.6 Problems with the photometric data

Having obtained the photometry of the long and short exposure the first thing was to check the data for consistency. Figure 2.1(a) shows the visual magnitude comparison of the short exposure and long exposure data sets. As can be seen, the visual magnitudes agree fairly well except for three stars that lie above the 1:1 line. Figure 2.1 (b) shows a comparison of the $V-I$ color indices. The stars fall slightly below the 1:1 line except for two distinct stars that lay above it. The scattering of stars below the 1:1 line shows that there is a systematic difference in the long and short exposure data sets. An attempt was made to try and rectify the problem because we intended to use the long exposure data for the photometric analysis because they are deeper images (thus fianter stars can be seen) than the short exposures. It was only realized later that the long exposure observation were faulty.

The first check on the data would obviously be the zero-points. Table 2.8 shows the zero-points for both the short aand long exposures. From this table it is obvious and apparent that the long exposures were faulty because of the relatively large error (43%) in the I-band zero-point. Also, a comparison of the zero-points of the long and short exposure zero -points show that the long exposure I-band zero-point is relatively high compared to the short exposure I-band zero-point.

1. An attempt was made to try and bring the sets of data into harmony, but it was later realised that this attempt was flawed.

2. After all this exercise, it was decided that the short exposures (without the modified zero-points) are the best to work with.

2.7 Summary

Cleaning of the data was successfully done with no problems. The photometric reductions went quite well except for the problem with the systematic difference that was observed between the short and long exposure data sets. It was realised that the long exposure observations were

Table 2.6: **The instrumental magnitudes of the standard stars.**

Star	FILTER	OTIME	AIRMASS	MAG	ERROR (MAG)
E417	*V*	21:20:11.0	1.028	13.290	0.002
	I	21:28:36.0	1.028	13.994	0.002
	R	21:25:10.0	1.028	12.998	0.001
	B	21:12:40.0	1.028	13.449	0.001
	U	21:05:52.0	1.028	15.923	0.002
E4103	*V*	21:52:29.0	1.024	13.075	0.002
	I	21:59:14.0	1.025	12.576	0.002
	R	21:55:58.0	1.024	12.202	0.001
	B	21:48:20.0	1.023	14.487	0.001
	U	21:42:22.0	1.022	18.403	0.005
E519	*V*	23:40:19.0	1.031	13.503	0.002
	I	23:47:09.0	1.030	13.937	0.002
	R	23:44:04.0	1.030	13.078	0.001
	B	23:32:17.0	1.033	13.897	0.001
	U	23:27:05.0	1.034	16.239	0.002
E607	*V*	01:20:51.0	1.066	12.489	0.001
	I	01:32:57.0	1.056	13.300	0.002
	R	01:25:17.0	1.062	12.203	0.001
	B	01:16:56.0	1.069	12.513	0.001
	U	01:12:04.0	1.074	14.960	0.001
E394	*V*	18:55:59.0	1.037	12.327	0.001
	I	19:04:29.0	1.041	15.404	0.008
	R	19:02:18.0	1.040	12.026	0.002
	B	18:52:00.0	1.035	13.857	0.001
E424	*V*	20:51.18.0	1.025	12.326	0.001
	I	20:51:18.0	1.025	12.749	0.001
	R	20:48:43.0	1.025	11.924	0.001
	B	20:44:36.0	1.026	13.095	0.001

This table gives the instrumental magnitude (MAG) and airmasses of the observed standard stars in the different bands (U, B, V, R and I) together with the time (OTIME) at which these observations were made. Stars E417, E4103, E519 and E607 were observed on the same night as the short exposure while E394 and E424 were observed on the same night as the long exposures. The table is self explanatory.

Table 2.7: **The zero points.**

Source	C_U	C_B	C_V	C_I	C_R
E417	5.40	3.37	3.11	4.59	4.43
E4103	5.38	3.40	3.56	4.64	3.52
E519	5.33	3.32	3.53	4.60	3.43
E607	5.38	3.33	3.45	4.60	3.39
E394	-	3.36	3.54	8.39	4.15
E424	-	3.82	3.67	4.74	3.60

Table 2.8: **The zero-points and their errors .**

	C_U	C_B	C_V	C_R	C_I
Short Exposure	5.37±0.03	3.35±0.03	3.40±0.20	3.82±0.40	4.61±0.02
Long Exposure	-	3.60±0.30	3.60±0.09	3.9±0.40	7.00±3.00

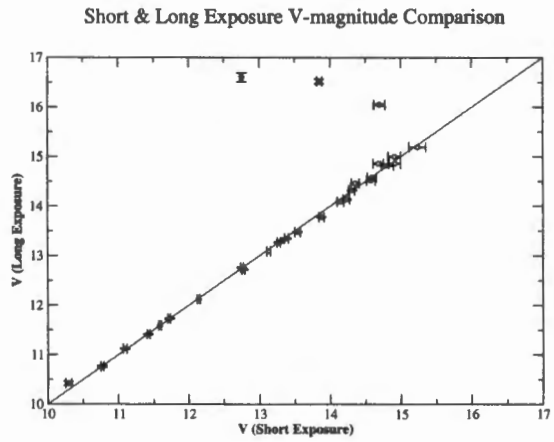

(a) This graph shows the visual magnitude comparison of the short exposure and long exposure data sets. As can be seen, the visual magnitudes agree fairly well except for three stars that lie above the 1:1 line.

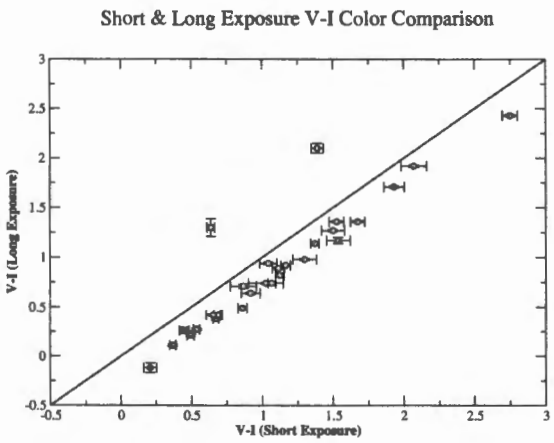

(b) This graph shows the comparison of the $V - I$ color indices of the short exposure and long exposure data sets. The stars fall slightly below the 1:1 line except for two distinct stars that lay above it. The scattering of stars below the 1:1 line shows that there is a systematic difference in the long and short exposure data sets.

Figure 2.1: The comparison graphs.

faulty and thus are not the best to work with, hence the short exposures UBV photometry has been used for this study.

Chapter 3

Cluster search in the field of G264.29+1.47

3.1 Introduction

In order to search for clusters, some objective measure of clustering must be used. A common way of searching for clustering in galaxies on a cosmological scale is by using the two-point correlation function first introduced by M. Totsuji and T. Kihara in 1969 (Peebles, 1980) and popularized by Peebles in the early 1980s (Hermit *et al.*, 1996). In this chapter the two-point correlation function will be introduced and applied to the field of G264.29+1.47.

3.2 The two-point correlation function

Following the discussion of Hermit *et al.* (1996) and Peebles (1980), the two-point correlation function $\xi(r)$ provides a measure of density excess over that expected for a random distribution of sources on a given scale length (say r) for a large scale distribution of galaxies or stars.

Consider a star to be a point in space. Then, given a distribution of points in space whose mean density is $\langle n \rangle$ and a volume element dV, the probability δP that a point is found anywhere in this volume dV is given by

$$\delta P = \langle n \rangle \, dV. \tag{3.1}$$

Now consider a uniform Poissonian distribution of points in space. The joint probability that a point is found in one of the two independent volume elements dV_1 and dV_2 scales with the mean density and the size of the elements. Thus it follows that

$$dP = \langle n \rangle^2 \, dV_1 dV_2. \tag{3.2}$$

If the distribution is non-Poissonian, then there is an excess probability of finding a point in each of the two volume elements dV_1 and dV_2 separated by the distance r, thus we can write

$$dP = \langle n \rangle^2 \, dV_1 dV_2 \, [1 + \xi(r)] \, . \tag{3.3}$$

This excess probability, quantified by $\xi(r)$, is known as the two-point correlation function. If the correlation function is negative, that is $-1 \leq \xi(r) < 0$, this means the objects are anti-correlated, that is, the likelihood of finding one object is diminished by the presence of another one. When the correlation function is positive and large so is the likelihood of finding one object next to another.

Since the probability of finding an object in dV_1 is $\langle n \rangle \, dV_1$, the conditional probability of finding an object in dV_2 given that there is an object in dV_1 is

$$dP(2|1) = \langle n \rangle \, dV_2 [1 + \xi(r)]. \tag{3.4}$$

Another way to put this is, if an object is chosen at random from an ensemble, the probability of finding that it has a neighbour at a distance r in dV is

$$dP = \langle n \rangle \, dV [1 + \xi(r)]. \tag{3.5}$$

Now the mean number of neighbouring points $\langle N \rangle_p$ within distance r of a randomly chosen point is the integral of equation (3.5), that is

$$\langle N \rangle_p = \frac{4}{3} \pi r^3 \langle n \rangle + \langle n \rangle \int_0^r \xi(r) dV. \tag{3.6}$$

For a Poisson distribution, $\xi = 0$, and the two means agree because of the fact that V has been centered on the point of interest does not affect the chance of finding objects anywhere else in V. If the positions are correlated, it does not bias the mean: the integral of equation (3.6) is the mean number of neighbours in excess of what is expected for a uniform random distribution.

If we extend the integral of equation (3.6) to all r, it gives the total number of neighbours in excess of the random distribution, that is

$$n_c - 1 = \langle n \rangle \int \xi dV \tag{3.7}$$

where n_c is the measure of the number of objects per cluster if the integral converges.

For example, suppose all objects are members of clusters, each cluster having diameter D and each containing n_c members, and suppose the cluster centers were distributed like a uniform

random Poisson process. Having chosen an object at random, one has also chosen the cluster to which it belongs. Since the clusters are supposed to be randomly distributed, this does not bias the distribution of other clusters, so they contribute $\langle n \rangle V$ to $\langle N \rangle_p$, the same as for a randomly placed volume. There are in addition $n_c - 1$ neighbours from the chosen cluster, so the integral $\langle n \rangle \int \xi dV$ is $n_c - 1$. If the number of objects per cluster is a random variable, the probability of choosing an object from a cluster with n_s members is proportional to n_s, so

$$\langle n \rangle \int_V \xi(r) dV = \frac{\langle n_s(n_s - 1) \rangle}{\langle n_s \rangle} \tag{3.8}$$

where the average is over the abundance of clusters in space. Equation (3.8) gives a method of calculating $\xi(r)$. Traditionally $\xi(r)$ has been determined by the expression

$$\xi(r) = \frac{DD(r)}{RR(r)} - 1 \tag{3.9}$$

where $DD(r)$ and $RR(r)$ are, respectively, the number of data-data and random-random pairs with separation within the range r and $r + dr$ from the chosen point. The latter is computed by creating a catalogue of randomly distributed points within the same volume occupied by the data points. In this dissertation $\xi(r)$ is referred to as the simple estimator. Although there are also other estimators for the two-point correlation function, our aim was not to do a comparative study of these estimators.

3.3 Monte Carlo simulations

We have a tool, namely the two-point correlation function, which can be used to detect clusters of stars or galaxies for a given distribution of stars and galaxies respectively. Before this tool can be used, it is wise to first test for its validity and how it works. Blindly applying the two-point correlation function without first testing it is unwise, because it would be difficult to interpret the results derived from it. This section crudely tests this tool, thus defining its validity and limits.

Intuitively it is expected that the two-point correlation function depends on the scale length (r_0) of the clustering. The two-point correlation function is not expected to be equally sensitive on all length scales of clustering and this must be investigated before applying it to the present data. Besides scale length sensitivity, it is possible that $\xi(r)$ might be sensitive to different distributions of stars with different relative numbers of cluster members and field stars. In the following paragraphs these issues are looked into and some of the important parameters which $\xi(r)$ is sensitive to will be established.

For simulation purposes a symmetric two-dimensional Gaussian distribution will be used to

generate a cluster. The scale length of the clustering will be taken as the standard deviation of this two-dimensional Gaussian. By scale length, it is understood that this is the standard deviation of the star's distance from the center of the Gaussian cluster and for the present purposes it is given in pixels. The computer code **C2** given in the Appendix has been used to generate the two-dimensional Gaussian clusters of stars of a given scale length, number of cluster members together with a random distribution of field stars. By varying one of the parameters while keeping the rest constant, the behaviour of $\xi(r)$ is determined ($\xi(r)$ will be ploted on the y-axis and will be labelled epscilon). The stars where placed on a 2048 pixel $\times$ 2048 pixel grid which is similar to the size of the Dandicam CCD chip.

1. Firstly the cluster scale length is varied while keeping the total number of field stars constant at 299 stars and the cluster members constant at 20 stars. The choice of 299 stars has been made on the basis of the fact that the real data on which the two-point correlation will be applied has a total of 299 stars. Setting the number of random stars equal to the actual number of stars in the real data is also done to avoid any density contrast. Figure 3.1 shows the dependence of $\xi(r)$ on the scale length of the cluster. The Random-Random Data graph shows how $\xi(r)$ varies for a purely random distribution of stars. Inspection of the Random-Random Data graph shows that $\xi(r)$ fluctuates around zero as intuitively expected.

2. If for some distribution of points there is a non-Poissonian distribution on a given scale, say r_0, then this shows up as deviations above the Random-Random Data graph within the scale length r_0. From figure 3.1 it can be seen that $\xi(r)$ depends on the scale length r_0 and picks the cluster more accurately the more compact the cluster is. For the present, it seems as if 500 pixels is the largest cluster size that $\xi(r)$ can accurately pick.

3. Table 3.1 shows a comparison of the "true" cluster scale length with the size determined by $\xi(r)$. Column 1 is the "true" scale length of the cluster and column 2 is the size of the cluster as determined by $\xi(r)$. It is apparent that $\xi(r)$ does pick the cluster roughly at the correct size, that is, at about 5 times its "true" scale length. From this it can be said (roughly) that the true scale length of the cluster is about 1/5 the size of the cluster as determined by $\xi(r)$. This kind of behaviour is intuitively expected because as was mention earlier, the "true" scale length is nothing but the standard deviation of the distance of the cluster stars from the center of the cluster and this standard deviation is roughly speaking about 1/5 of the diameter of the cluster. This relation is true for Gaussian distributions.

4. Figure 3.2 shows the variation of $\xi(r)$ with the number of cluster members. The total number of stars in the field is kept constant at 299 while varying the number of cluster members as a percentage of the total number of stars on the field. The scale length

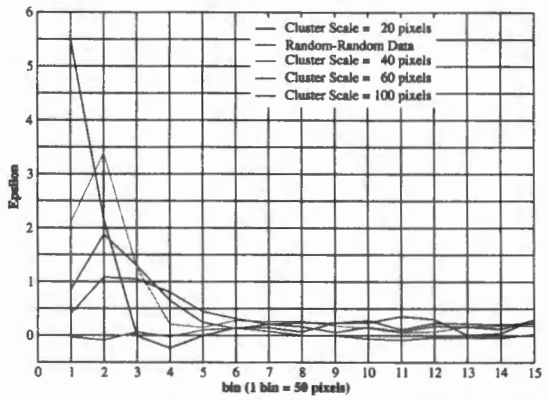

Figure 3.1: Monte Carlo simulations showing the variation of $\xi(r)$ with the **scale length of the cluster**. The number of cluster members was kept at 20 while the cluster scale length was varied from 20 pixels to 100 pixels.

Table 3.1: **Comparison of the actual cluster scale length to that determined by** $\xi(r)$

Cluster Scale length (pixels)	**Scale length as determined by** $\xi(r)$(pixels)
20	~150
40	~200
60	~300
100	~450

of the cluster was kept constant at 50 pixels. It can be seen from the graph that the ability to detect the cluster depends rather strongly on what percentage the number of cluster stars is of the total number of stars considered. The more the cluster members, the better $\xi(r)$ indicates the presence of a cluster.

5. Figure 3.3 shows the dependence of $\xi(r)$ on the total number of stars on the field with the number of cluster stars kept constant at 60. As the number of field stars increases the cluster becomes difficult to detect. With 900 stars on the field, the cluster almost escapes detection with $\xi(r)$ almost behaving like the Random-Random Data case. It is clear from this that one must take care if he/she is to detect the cluster using the two-point correlation functions. If the exposure time is too short, too few stars are seen on the CCD and if the exposure time is too long, too many stars appear and this may obstruct one from seeing the cluster.

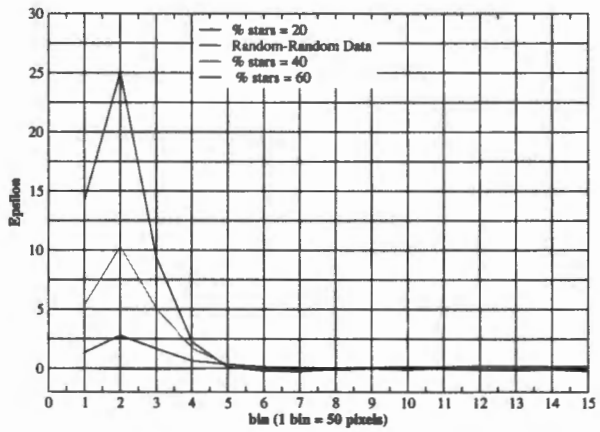

Figure 3.2: Monte Carlo simulations showing the variation of $\xi(r)$ with the number of **cluster stars**. The cluster scale length was kept constant at 50 pixels and the number of cluster members varied from 20% to 60% of the total number of stars on the field. The number of field stars was kept at 299.

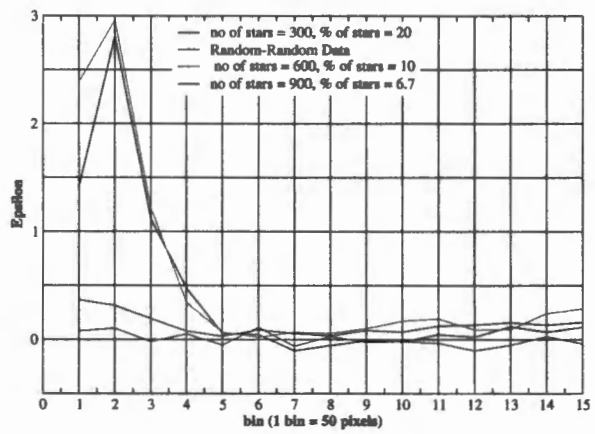

Figure 3.3: Monte Carlo simulations showing the variation of $\xi(r)$ with the number of **field stars**. The cluster scale length was kept at 50 pixels and the total number of stars on the field was varied from 300 to 900 while the number of cluster members was kept constant at 60 stars, hence the variation in the % of stars.

3.3.1 The behaviour of $\xi(r)$

The following can be said about the dependance of $\xi(r)$ on parameters such as scale length of the cluster, the number of field stars and the number of cluster members on the field.

1. The simple estimator is sensitive to a non-Poissonian two-dimensional distribution of stars and is capable of determining the scale length at which this distribution occurs. However, it is not equally sensitive on all scales. For the present study it appears to be accurate for scale lengths of less than 500 pixels. Since the CCD is a 2048 pixels $\times$ 2048 pixels field, a more general statement about the scale length determination is that the ratio of the cluster size to that of the field must be less than 0.24 for the cluster to be detected fairly well, that is, about 500 pixels (for maximum reliable scale length) divided by 2048 pixels (the size of the field), which gives 0.24.

2. As for the determination of the scale length, the simple estimator appears to be rather insensitive to the number of cluster members for a given number of stars on the frame. Only the maximum value of $\xi(r)$ increases with increasing number of cluster members for a fixed number of stars, but for the purposes of this dissertation, it is not important, hence attention will not be paid to this.

3. The simple estimator appears to be sensitive to the number of cluster stars relative to the number of field stars. For a given distribution of stars with the number of cluster stars kept constant while the number of random field stars is increased, $\xi(r)$ gradually begins to behave like that of a random distribution of stars. This means that as the random field stars are added, the cluster escapes detection.

4. A point to note is that it can happen that there is more than one cluster in a particular region. Intuitively one could expect that the size of clustering determimed by the two-point correlation function will be that of the largest cluster. This claim has not been simulated. In a case like this, we can only talk of the maximum size of clustering in this region for each of the clusters. As will be seen later, there are two clusters detected in the field of G264.29+1.47.

3.4 Application of the two-point correlation function on the field of G264.29+1.47

The I-band frame contains the largest number of stars of the field of G264.29+1.47. A total of 299 stars are visible on this frame. The positions of these stars were used to compute $\xi(r)$. Figure 3.4 shows the distribution of the stars as seen on the CCD frame.

The program code **C1** given in the Appendix was used to calculate $\xi(r)$ for the field of G264.29+1.47. Using Monte Carlo simulations, 100 random catalogues of 299 stars were generated. The number of random stars was made equal to the number of data stars to avoid any density contrast fluctuations hence the choice of the 299 stars as for the Monte Carlo simulations. For each of the catalogues, $RR(r)$ was calculated in the same way as $DD(r)$ and hence $\xi(r)$ was calculated. This gave rise to 100 values of $\xi(r)$, from which an average and the standard deviation were computed. The standard deviation was used as a measure of the error in $\xi(r)$. There is no standard method of estimating the error and any reasonable method can be used as a measure of the error (Hermit *et al.*, 1996).

Figure 3.5 shows the two-point correlation function for the field of G264.29+1.47 from the 2001 observations. From this graph, it is apparent that $\xi(r)$ deviates from that expected for a random distribution of stars and this suggests the presence of some degree of clustering. From this graph, the size of the cluster is approximately 200 pixels. As was mentioned in section 2.3.1, the plate scale of the CCD is 0.28 arcsec/pixel, hence the real size of the clustering in this field is approximately 56 arcsec.

Figure 3.6 shows the two-point correlation function for the same region but this time with more stars appearing on the field. This is from the 2002 observations where the integration time was increased from $\sim 30\,s$ (for the 2001 observations) to $\sim 600\,s$, so more faint stars could be seen. From this graph, there appears to be no clustering at all. We know from the Monte Carlo investigations (from behaviour **(3)** (section 3.3.1) of $\xi(r)$), that the 2002 observations included many random field stars which obstructed the cluster from being detected.

3.5 Locating the position of the cluster

Having established the presence of at least one cluster, the next task is to find where this cluster is located on the CCD image. This task is accomplished by applying the auto-correlation function to the field. The auto-correlation function is a conventional measure used for detecting spatial irregularities across a field (Lang, 1999).

Suppose we divide the sky as seen on the CCD frame into equal area cells as shown in figure 3.4, then the auto-correlation function is defined as

$$\xi_A(r) = \frac{\langle \rho(r_1)\rho(r_1+r)\rangle}{\langle \rho \rangle^2} - 1 \tag{3.10}$$

where $\rho(r_1)$ is the mean density of a cell located at position r_1. For a given distribution of points, $\xi_A(r)$ can be estimated from the function (Peebles, 1980)

$$\xi_l(i,j) = \frac{\sum_m \sum_n \langle n \rangle_{ij} \langle n \rangle_{mn}}{\langle n \rangle^2} - 1 \tag{3.11}$$

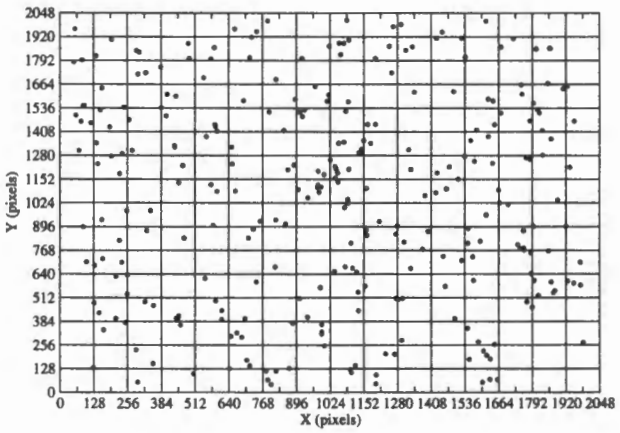

Figure 3.4: The positions of the stars as seen on the I-band CCD frame. This data is from the 2001 observations. A total of 299 stars appear on this frame.

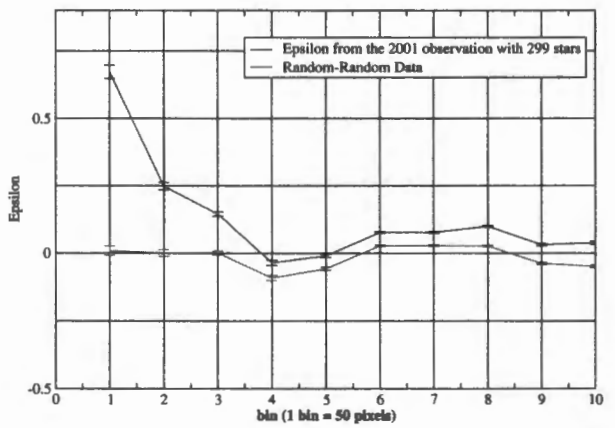

Figure 3.5: The two-point correlation function for G264.29+1.47. This has been obtained from the 2001 observation data with a total of 299 stars appearing on the I-band CCD frame as seen in figure 3.4.

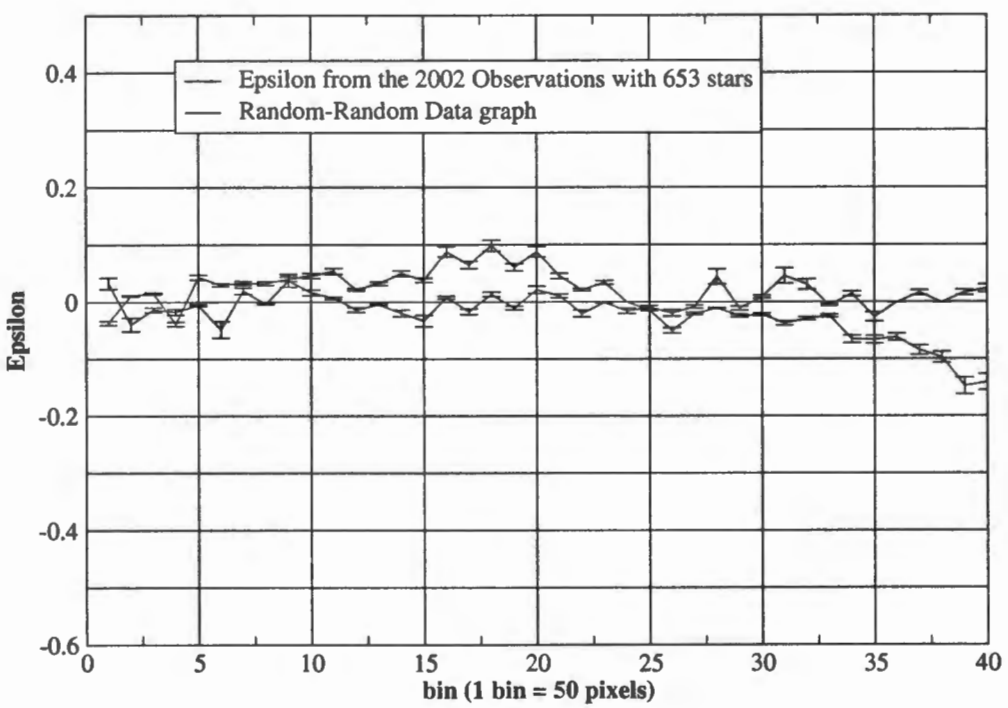

Figure 3.6: The two-point correlation function for G264.29+1.47 from the 2002 observations with a total of 653 stars appearing on the I-band CCD frame.

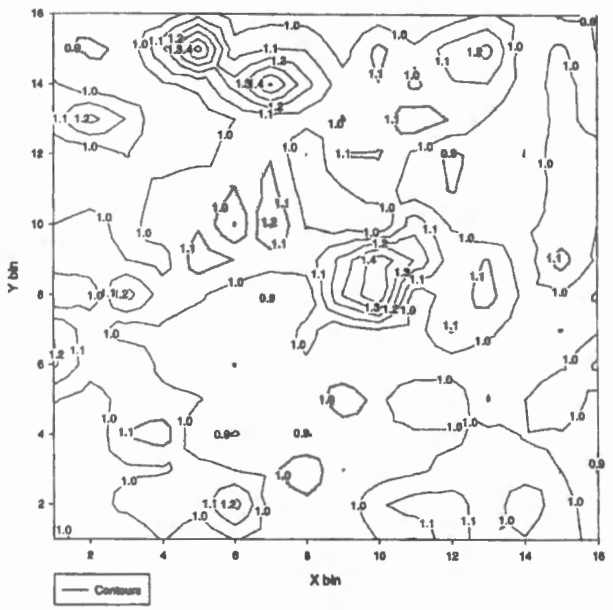

Figure 3.7: The contour map of the auto- correlation function for the field of G264.29+1.47. At the center of this figure it can be seen that ξ_l has a maximum value there of ~ 1.4. This position coinsides with the nebulosity.

where r is the distance of separation of the cells and $\langle n \rangle$ is the mean density of the stars on the whole CCD frame. $\xi_l(r)$ is high where the cluster centre has a high probability of being located, because the spatial irregularities are centered around this point. $\xi_l(r)$ is low where the cluster center is least expected to be located.

For the field of G264.29+1.47, $\xi_l(r)$ was computed using the program code **C4** given in the Appendix A. A contour map of the auto-correlation function is shown in figure **??**. It is seen that $\xi_l(r)$ peaks around two regions in this field, the peak value being 1.4. Intuitively one would have expected the peak in the centre of the field which is associated with the nebulosity which also is the region of star formation. The second peak is in the upper part of the field. Given the fact that the auto-correlation function did locate the central cluster, there is no reason to believe that the upper cluster is an artifact. The upper cluster will here after be refered to as the upper cluster and the central cluster associated with nebula as central cluster

.

3.6 Discusion

The presence of the upper cluster came as a surprise. Would the field have been smaller, the upper cluster would not have been detected.

Two questions immediately come to mind: (1) are the two clusters related in anyway to the same molecular cloud ? and (2) is there an age difference between the two? The present

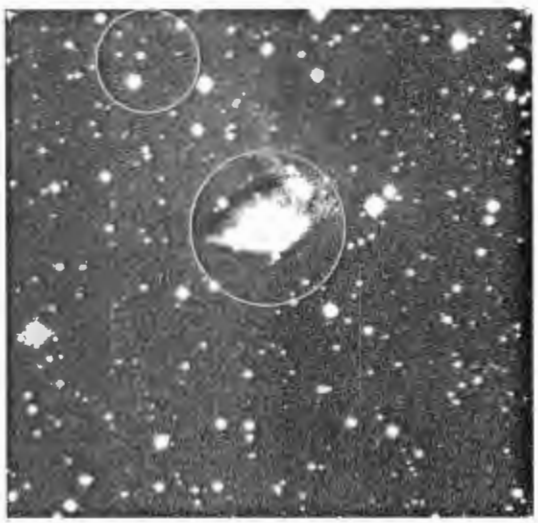

(a) The R-band image of G264.29 +1.47. The two circles show the position of the two clusters. The nebulosity is seen to stretch from the central cluster towards the upper cluster .

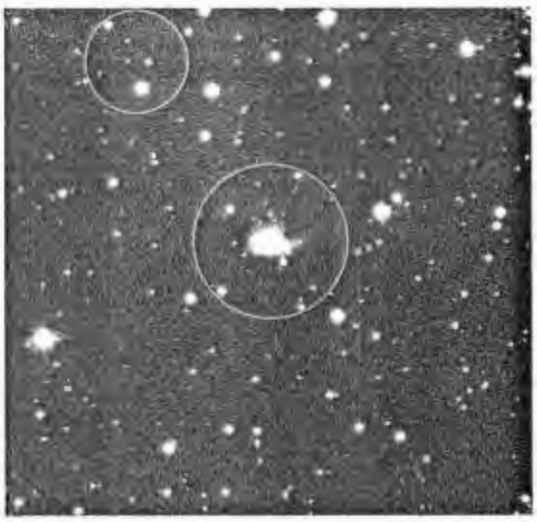

(b) The I-band image of G264.29 +1.47. The nebulosity is visible but not as visible as in the R-band.

Figure 3.8: The I and R band images of G264.29 +1.47. These images were take from the 2002 observations. **Note:** The size of the circles are not indicative of the size of the cluster.

observations cannot give a definate answer to any of these questions. However we note the following from the images at hand.

Figure 3.8(a) shows the R-band image of this region. In R-band, the distribution of the nebulosity is best seen and it is seen that there appears to be evidence of the nebulosity linking the cenrtral region with the upper cluster. This strongly suggest that the molecular cloud must have extended to the upper part of the field. The absence of any strong nebulosity associated with the upper cluster might suggest that the upper cluster is slightly older than the central cluster, having already cleared away most of the gas through the joint action of stellar winds of stars in the cluster. These qualitative ideas, however, have to be tested by more detailed optical, near-infrared and molecular line observations.

3.7 Summary

The two-point correlation function has been discussed and briefly studied by Monte Carlo simulations. It has been found that it depends on the scale length, number of cluster stars and field stars. By noting its behaviour, some of the cluster properties of the field of G264.29+1.47 have been deduced. Having applied the two-point correlation function and the the auto-correlation function to the field of G264.29+1.47, it is concluded that there are two clusters in this field, a central cluster around the nebula and a cluster in the upper part of the field. The size of clustering in this field $\sim$ 56 arcsec.

There is need to extend the present observations to the near-infrared and milimeter or sub-milimeter obseravtions and combine them with optical ones to establish any correlation (if any at all) between the two clusters. This correlation is of importance insofar as star formation is concerned in this region.

Chapter 4

Photometric analysis of G264.29+1.47

4.1 Introduction

The discovery in the early 20th century independently by astronomers Ejnar Hertzsprung and Henry Norris Russell of the now-called Hertzsprung-Russell (H-R) diagram (whose modern equivalent is the color-magnitude diagram), is probably the greatest observational synthesis of all in Astrophysics. These diagrams have been used to study the nature of stellar populations. The H-R diagrams are probably the most powerful tools available to any stellar astronomer today. In this chapter an attempt is made to analyse the photometric data of stars of the field of 264.29+1.47 H-R diagrams. The aim of this attempt is to gain some practical experience with this type of analysis. Central to this analysis will be to deredden some of the stars inorder to estimate spectral types.

4.2 The Photometry tables

Table 4.1 lists the UBV photometry of 28 stars detected simultaneosuly in the three bands U, B , and V respectively. Column 1 lists the label of the stars as shown in figure 4.1. Columns 2 and 3 list the X and Y pixel coordinates of these stars as seen on the CCD frame. Column 4 lists the visual magnitudes of these stars and column 5 the corresponding errors. Columns 6, 7, 8 and 9 list the $B-V$ and $U-B$ colors of the stars together with the corresponding errors respectively.

Inspection of the photometry table shows that the visual magnitudes of these stars ranges from about 11 to 15 mags. This means these are relatively faint sources, thus for better photometry we need relatively longer integration times. The errors in the colors and visual magnitudes range between 0.01 to 0.09. These errors were obtained directly from the **IRAF** software.

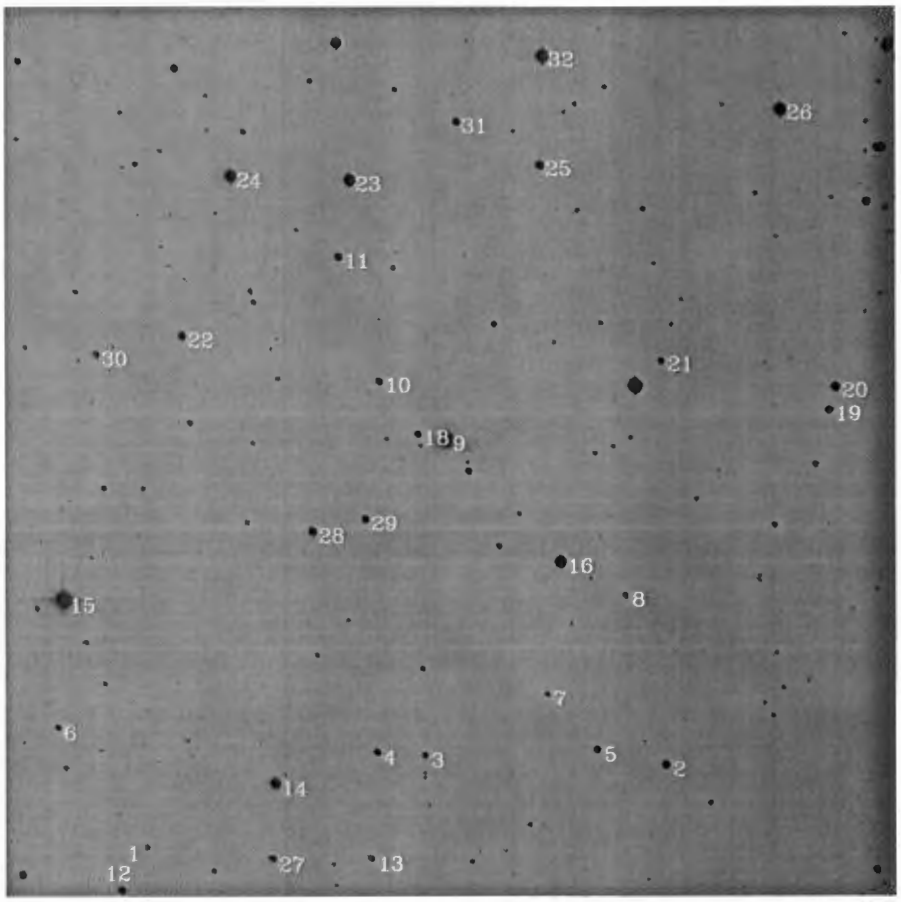

Figure 4.1: The short exposure image of the field of G264.29+147.

Table 4.1: **Short Exposure *UBV* Photometry**

Star	X	Y	V	ΔV	$B-V$	$\Delta(B-V)$	$U-B$	$\Delta(U-B)$
2	1531.84	389.89	13.85	0.02	0.60	0.03	0.11	0.01
3	977.52	410.95	15.02	0.04	1.26	0.05	1.06	0.09
4	867.29	418.28	14.57	0.04	1.13	0.04	1.04	0.06
5	1374.42	425.16	14.67	0.04	0.72	0.05	0.18	0.05
6	133.35	473.77	15.63	0.09	1.05	0.09	0.46	0.08
9	1027.79	1139.62	11.48(0)	0.00(2)	0.80(0)	0.00(2)	-0.13(0)	0.00(2)
10	872.42	1274.06	14.95	0.04	0.91	0.05	0.24	0.04
11	778.77	1559.18	14.10	0.03	0.83	0.03	0.57	0.02
12	226.80	52.28	15.20	0.06	1.12	0.06	0.63	0.07
14	633.02	345.90	12.85	0.02	0.38	0.02	0.03	0.01
15	147.26	766.99	11.01	0.04	0.08	0.05	0.00	0.03
16	1291.23	857.81	12.31	0.02	0.47	0.02	0.14	0.01
17	1078.35	1068.19	15.29	0.06	0.66	0.06	0.48	0.06
18	960.60	1152.61	15.41	0.08	0.88	0.08	0.21	0.05
19	1905.05	1207.99	14.82	0.05	0.59	0.05	0.15	0.03
20	1920.63	1260.88	13.47	0.02	0.70	0.02	0.61	0.02
21	1520.51	1320.97	15.31	0.07	1.12	0.07	0.29	0.06
22	419.32	1377.23	14.59	0.04	0.82	0.04	0.52	0.04
23	804.96	1735.05	12.14	0.02	0.22	0.02	0.07	0.01
24	531.56	1743.66	12.44	0.02	0.21	0.02	0.31	0.01
25	1242.74	1770.22	13.47	0.02	0.34	0.03	0.05	0.01
26	1794.29	1898.55	11.81	0.03	1.15	0.03	0.92	0.01
27	626.10	171.72	15.07	0.06	1.28	0.06	0.90	0.10
28	718.83	926.45	13.49	0.02	0.46	0.02	0.09	0.01
29	840.80	955.30	14.25	0.04	0.48	0.04	0.09	0.02
30	221.49	1334.17	15.40	0.08	1.05	0.08	0.44	0.07
31	1050.43	1869.05	13.99	0.02	0.89	0.03	0.19	0.03
32	1249.08	2019.82	11.48	0.02	0.42	0.02	0.07	0.02

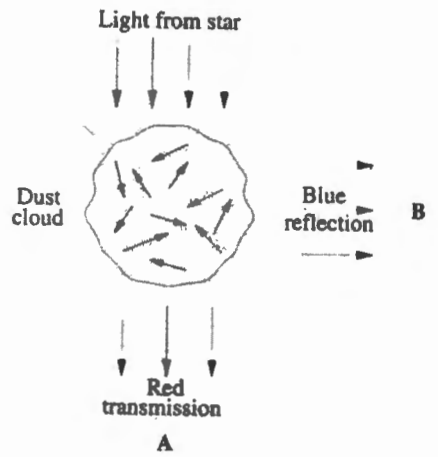

Figure 4.2: A dust cloud can either scatter or absorb light that passes through it. The amount of scattering and absorption depends on the number density of particles, the wavelength of light and the thickness of the cloud. Since shorter wavelengths of light are affected more significantly than longer ones, a star lying behind the cloud appears reddened to observer A. Observer B sees the scattered shorter wavelength as blue reflection nebula. (Adapted from Modern Astrophysics by Bradley W. Carroll & Dale A. Ostilie page 439.)

4.3 Interstellar reddening

Before a photon reaches our planet from the stars, it must first pass through an absorbing medium. This medium is known as the interstellar medium. The interstellar medium consists mainly of gas and dust. The interstellar gas generally absorbs radiation at discrete, well defined frequencies, and therefore shows up as absorption lines in stellar spectra.

Interstellar dust scatters light over a much broader range of spectral wavelengths. The scattering is different for different wavelengths. It scatters blue light more than red light. As a result this makes a star appear more red than in the absence of dust, hence the term interstellar reddening. This modifies a star's color index (see figure 4.2) and hence the distance modulus of the star . The distance modulus of a star is given by

$$m - M = 5\mathbf{log}[d] - 5 \tag{4.1}$$

where m , M and d are the apparent magnitude, absolute magnitude and distance of the star from the Sun respectively. In the presence of extinction, the distance modulus is modified and re-written as

$$m - M = 5\mathbf{log}[d] - 5 + A_\lambda \tag{4.2}$$

where A_λ represents the amount of absorption at a wavelength λ.

Since reddening modifies the color index, a quantity called the color excess CE can be defined, that is if the intrinsic color index is CI_i and the observed color index is CI_o, then

$$CE = CI_o - CI_i. \tag{4.3}$$

The intrinsic color index depends on the spectral type of the star and is determined from its spectrum or by examining the $U-B$ vs $B-V$ color diagram as was done in this study. The spectral type of a star is most reliably determined by spectroscopy. Determination of spectral type by means of a color-color diagram is somewhat uncertain because at times more than one solution of spectral type is obtained, as will be shown later.

4.4 Dereddening

The process of correcting for the interstellar reddening is called dereddening. In order to deredden a star, one must first establish a dereddening law; fortunately it is not difficult to do that. The dereddening law is an algorithm used to obtain the intrinsic colors of a star. This algorithm incorporates in it the so-called reddening vector. The derredening law is not the same for all stars (van den Ancker *et al.*, 1996) and this must checked if one really needs very accurrate measurements. For a thorough study of this region one needs to check the derredening. In the following paragraph the reddening process will be discussed.

Consider a star of intrinsic color indices $(U-B)_0$ and $(B-V)_0$ which has apparent color indices $(U-B)$ and $(B-V)$ respectively. The $U-B$ and $B-V$ color excess $E(U-B)$ and $E(B-V)$ are defined as

$$E(U-B) = (U-B) - (U-B)_0 \tag{4.4}$$

$$E(B-V) = (B-V) - (B-V)_0 \tag{4.5}$$

respectively. Observations indicate that

$$\frac{E(U-B)}{E(B-V)} = \gamma \tag{4.6}$$

and

where γ is practically constant (Zeilik & Gregory, 1998; Bowers & Deeming, 1984) and for this study it was taken to be 0.72 (van den Ancker *et al.*, 1996). Assuming all the stars are main-sequence stars, then the reddening vector gives the direction in which the color index of the star is shifted from the main-sequence curve to where it appears. This shift is due to interstellar extinction. Having derredened the stars, we know the color excess, and knowing

the color excess the visual extinction A_V can be estimated from the approximate equation (Zeilink & Gregory, 1998; Bowers & Deeming, 1984)

$$A_V \sim RE(B-V) \tag{4.7}$$

where $R \sim 3$.

Figure 4.3 shows the $U-B$ vs $B-V$ graph that was used for the dereddening. The stars on this graph lie along the main-sequence curve of Schmidt-Kaler (1982) (The Schmidt-Kaler main-sequence has been plotted using the values shown in table 4.2). Using interpolation methods the main-sequence curve was approximated by a sixth order polynomial

$$y = ax^6 + bx^5 + cx^4 + dx^3 + ex^2 + fx + g, \tag{4.8}$$

where $y = U-B$, $x = B-V$, a $= 8.94$, $b = -27.54$, $c = 23.51$, $d = 0$, $e = -7.66$ and $f = -2.58 \times 10^{-2}$. The reddening vector for each star is given by the equation

$$y = \gamma x + q_i, \tag{4.9}$$

where q_i is the $U-B$ intercept on the $U-B$ vs $B-V$ for each star. Equating equation 4.8 to equation 4.9 and after some algebra manupulation, we get

$$0 = ax^6 + bx^5 + cx^4 + dx^3 + ex^2 + (f-\gamma)x + (g-q_i). \tag{4.10}$$

The solution to this equation for each of the stars was obtained using the Newton-Raphson method. The computer code **C3**, given in the Appendix, was used to perform the task of computing the solutions to equation 4.10.

4.5 Results

Table 4.3 lists the results obtained from the dereddening of the observed short exposure stars. Columns 2 lists the derived spectral type of the stars. In most cases more than one solution is obtained due to the fact that the derreddening vector intersects the main-sequence at more than one point. In most cases, only the range of spectral types of stars for a single solution is given. This mainly stems from the fact that the empirical main-sequence is listed for only some spectral types. If the intersection between the dereddening vector and the main-sequence lies between two such listed spectral types, the spectral type of the star is assumed to lie in that range. Deriving the exact spectral type would require more accurate data than was available for this study.

Table 4.2: **The Empirical Schmidt-Kaler main-sequence**

Main-Sequence Stars (Luminosity Class V)		
Spectral Type	$U-B$	$B-V$
O5	-0.19	-0.33
O6	-1.17	-0.33
O7	-1.15	-0.32
O8	-1.14	0.32
O9	-1.12	-0.31
B0	-1.08	-0.30
B1	-0.95	-0.26
B2	-0.84	-0.24
B3	-0.71	-0.20
B5	-0.58	-0.17
B6	-0.50	-0.15
B7	-0.43	-0.13
B8	-0.34	-0.11
B9	-0.21	-0.07
A0	-0.02	-0.02
A1	0.02	0.01
A2	0.05	0.05
A3	0.08	0.08
A5	0.10	0.15
A7	0.10	0.20
A8	0.09	0.25
F0	0.03	0.03
F2	0.00	0.35
F5	-0.02	0.44
F8	0.02	0.52
G0	0.06	0.58
G2	0.12	0.63
Sun[a]	0.17	0.68
Sun[b]	0.16	0.64
G5	0.20	0.68
G8	0.30	0.74
K0	0.45	0.81
K1	0.54	0.86
K2	0.64	0.91
K3	0.80	0.96
K4	-	1.05
K5	0.98	1.15
K7	1.21	1.33

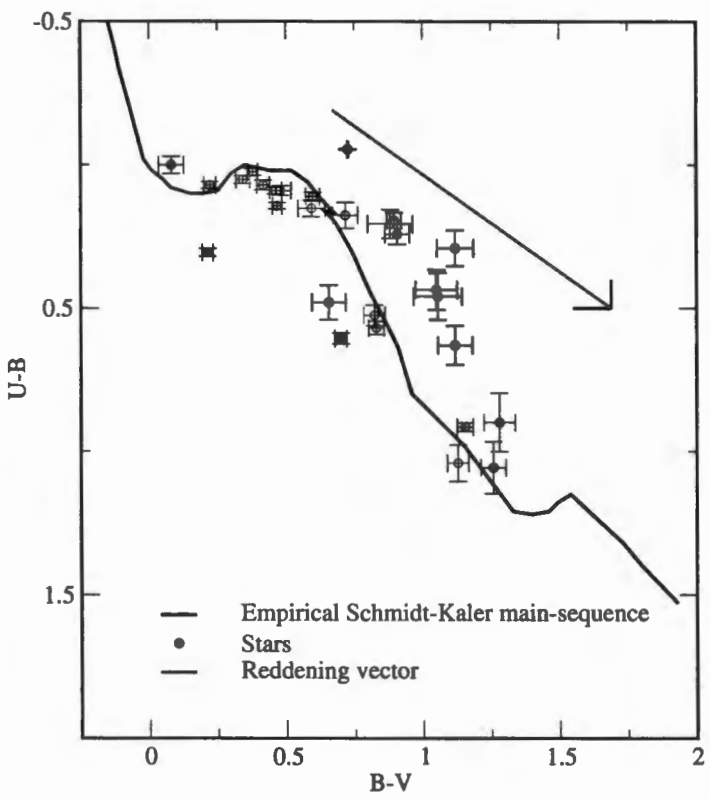

Figure 4.3: The $U-B$ vs $B-V$ color-color diagram. The reddening vector in this diagram runs from top to bottom. To deredden the stars, one simply moves the stars to the main-sequence line parallel to the direction of the reddening vector. The Schmidt-Kaler main-sequence has been plotted using the $U-B$ and $B-V$ values listed in table 4.2.

Table 4.3: **Distance, Color Excess & Possible Spectral Type of the Stars**

Star	Possible Spectral Type derived from the UBV colors	Minimum A_V	Maximum A_V	Maximum $E(B-V)$	Minimum $E(B-V)$
2	B7, F0, F8-G0	0.71	2.19	0.73	0.23
5	B7, F2, G0	1.03	2.57	0.87	0.34
6*	B6, F2, G2	2.11	3.54	1.18	0.70
7	B2	2.81	2.81	0.94	0.94
9*	B2	2.77	2.77	0.92	0.92
10*	B5	3.21	3.21	1.07	1.07
11	A0, A3	1.94	2.50	0.83	0.64
13	B8, A7, G5	2.51	3.59	1.20	0.84
14	F0, B7	0.17	1.46	0.49	0.06
15	B8, A7	0.31	0.31	0.10	0.10
16	B8-B9, A2	0.52	1.67	0.56	0.17
17	A2	1.54	1.54	0.51	0.51
18*	B5	3.14	3.14	1.05	1.05
19	B7, F0	0.77	2.14	0.71	0.26
21	B3	1.94	3.94	1.31	0.64
22	A0, A3	1.83	2.55	0.85	0.61
23	B8-B9, A7-A9	0.79	0.79	0.26	0.26
25	B8, A7	0.15	1.29	0.43	0.05
27*	B7, A8-F0	3.31	3.31	1.10	1.10
28	B7, A8-F0	0.43	1.71	0.56	0.15
29	B7, A8-F0	0.46	1.77	0.59	0.15
30	B7, G2, F2	2.06	3.55	1.18	0.68
31*	B5	3.21	3.21	1.07	1.07
32	B7, A7-A9	0.31	1.55	0.52	0.10

For stars that had one solution, the maximum color excess was set equal to the minimum color excesses, hence also the maximum and minimum visual extinction (for example star 17). This obviously has been made on the assumption that the normal extinction law holds. Columns 3 and 4 list the corresponding minimum and maximum visual extinctions as calculated from equation 4.7. Columns 5 and 6 list the minimum and maximum color excess.

Inspection of the spectral types shows that all the solutions give stars of spectral type earlier than A9 at the most. Although this may seem odd, it should be realised that this is based on the short exposure data and that one can therefore expect that only the brightest stars were detected. However, no attempt was made to see how these solutions agree with the predicted space densities of stars of various spectral classes in the solar vicinity. Obviously, to do any better than what has been done here it is necessary to determine spectral types with spectroscopic observations.

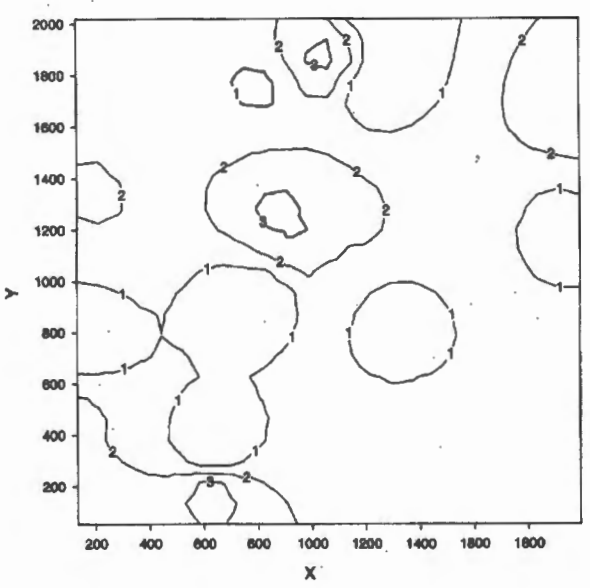

Figure 4.4: The extinction map of G264.29+1.47 from the 2001 observations.

4.6 The extinction map

The estimated spectral types and color excesses also allow a further check, albeit a relative one, on the data analysis. Assuming again a normal extinction law, it is possible to draw a crude contour plot of the visual extinction across the region covered by the image. For the present, only the maximum color excess and therefore the maximum extinction was used. The result is shown in figure 4.4. Inspection of this figure shows three regions where the visual extinction is about 3 magnitudes. The central region, however, is the largest and corresponds spatially almost with the nebulosity seen in most of the images. Direct correspondence is, however, not necessary since the distribution of the extinction can only be estimated towards those stars that were detected. Since only the data from the short exposures were used, it cannot be expected that the extinction in front of the fainter stars could also be determined. The other region of relatively high extinction is the upper and lower part of the field. In the vicinity of the upper cluster, no stars were detected in the U, B and V bands and hence nothing can be said about the extinction for this part of the field.

4.6.1 The central star

The central star's (star 9, see figure 4.1) UBV photometry and spectral type has been derived by Heydari-Malayeri (1988). This author gives $V = 11.81\pm < 0.03$, $B - V = +0.94\pm < 0.03$ and $U - B = -0.15\pm < 0.03$ and claims this star is a O8.5V zero-age main-sequence star located at a distance of 2.9 kpc. Contrary to claims made by Vittone *et al.* (1987), Heydari-Malayeri (1988) argued that this star is not a super-giant. In the present study, this stars

UBV photometry has been found to be, $V = 11.480 \pm 0.002$, $B - V = 0.800 \pm 0.002$ and $U - B = -0.130 \pm 0.002$ and the spectral type to be B2V. Regarding the extinction of this star Heydari-Maleyeri found $A_V \sim 4.2$ mag (and attributes it to local and interstellar dust) compared to our $A_V \sim 3.94$ mag. There is a significant difference between our results and those of Heydari-Malayeri in the spectral type and visual extinction of the central star. We cannot say our results are an improvement to those of Heydari-Maleyeri because we know our data is notof good quality. There is thus need to rework this with better quality data

Heydari-Malayeri further reports the presence of an ionisation front associated with a high velocity feature of ~ 100 kms^{-1} and suggests that this might be linked to the maser source. Beyond the ionisation front within this nebula this author claims a new star is being formed. This makes this region a very interesting one and worthy of further study. There is therefore need to make deeper imaging of this region and also carry out a thorough spectroscopic and photometric study of it.

4.7 Summary

A photometric study of the field of G264.29+1.47 has been carried out. Using 24 stars detected in the UBV bands, information such as possible spectral type of the stars and the nature this region regarding its extinction properties have been derived. The visual extinction has been found to be relatively high around the nebula region. The derived spectral type of the stars shows that the stars that were analysed are probably of spectral type earlier than A9. Spectroscopic observations of these stars is needed to accurately determine the spectral types and to verify the present estimates. It is concluded that there is need to make a thorough photometric and spectroscopic study of this region.

Chapter 5

Discussion and conclusions

5.1 Discussion

The aim of this study has been to search for optically visible clusters in selected high mass star formation regions associated with methanol masers. This has been achieved, we have detected a cluster in the field of G264.29 +1.47 that is associated with the methanol maser found in this region. Another cluster has been detected, that is the upper cluster and seems not associated with the maser. This cluster (the upper cluster) is of interest in as far as understanding star formation in this region if (at all) the two clusters have some form of association. The scale length of clustering in this region is of the order of 56 arcsec.

The techniques developed in this study of detecting clusters could have been applied on other regions as well, but due to time constraints this was so, thus, it is recomended that this technique be applied to these regions. To improve on the method, a thorough study of the two-point correlation function to galactic clusters is needed. There are other different estimators used to dectect clusters which are more sensitive than the simple estimator used here such as the Hamitonian estimator that has been used by Hermit *et al.* (1996). These estimators need to be tested and used for future search of clusters. It was not part of this study to make an in-depth study of the two-point correlation functions.

The broader scope of this study is to go beyond just detecting clusters associated with methanol masers but to also study the stellar content and star formation history of these clusters in the hope that this could give us some clues to the intriguing questions of how massive stars are formed. The first step in understanding star formaion history of any stellar population is by studying the region photometrically and spectrocopically. A brief photometric study of G264.29 +1.47 has been conducted. It is found that the detected UBV stars of this region are of spectral types earlier than A9V. This is however not surprising as it should be understood that this is based on the short exposure data and that one can therefore expect that only the brightest stars were detected. From the photometry of the stars, the extniction properties of

G264.29 +1.47 have been derived. The photometrically derived spectral types of stars need to be checked with some spectroscopically derived ones. This will also help in establishing whether the dereddening law is the same for all stars of this field.

It should be borne in mind that the photometric results of the present study are not to be relied on because the observations were not that good. This was pointed out in chapter two. There is thus need to observe anew with greater care than the previous observations. This however has been done by D. J. van der Walt in February of 2002. These observations (optical and spectroscopic) and are to be processed and it remains to be seen whether they are better than the 2001 observations.

On the prospects of studying this region further, this programe must continue as initially envisaged, that is, from the present observations (that is, optical observations), spectroscopic observations on the cluster members must be done (stated more precisely, possible cluster members) in order to determine the spectral types of as many as possible of the cluster members and thus also the distance modulus of the sources. We have good enough reasons: (1) we know there is a cluster; (2) we know there is at least a massive star in the process of formation through the associated 6.7 GHz methanol maser; (3) the existing facilities in South Africa allow for such work to continue and hence lay the ground work before more sophisticated instruments such as the Southern African Large Telescope (**SALT**) are operational.

5.2 Conclusions

From this study we present the following conclusions and recomendations:

1. From the cluster search conducted, we report detection of two clusters (the central and upper cluster) in the field of G264.29 +1.47. The central cluster seems to be associated with the methanol maser region while the upper cluster seems not. The size of clustering in this region is of the order of 56 arcsec.

2. There is need to make non-optical surveys and combine them with optical ones in order to make sense of the relationship between the two clusters detected.

3. Many of the stars detected (in the short exposure frames) appear to be of spectral type earlier than A9. However, this needs to be checked with spectroscopic measurements as well. Also, there is need to redo the photometry of the stars as these present observations were not good.

4. A thorough study needs to be undertaken to investigate how accurate the dereddening process is and therefore how accurately the spectral type can be determined photometrically. Also needed is a thorough study of the two-point correlations function.

5. Based on the positive detection of the clusters, it is concluded that it is worth extending this type of study to other star formation regions. The region G264.29+1.47 appears to be worth studying in more detail. It is hoped that the experience gained and lessons learnt will greatly improve in the next phase of the project.

Appendix

Program Code C1

/**********/This computer code is designed to calculate the two point correlation function for a given set of co-ordinates ($0 \leq x \leq 2048$ and $0 \leq y \leq 2048$).The code reads data from the file tvi which has three columns, where column one and two are the x and y co-ordinates and the third column are the instrument magnitude of the stars corresponding to the x and y co-ordinates. The program asks the user for the number of experiments which is the number of random catalogue of stars for the Monte Carlo simulations. It out puts that results in the three out put files mcoutfile.txt, mc-data-outfile.txt and mc-mc-outfile.txt. For the purpose of this study only those results out put in to the file simple.txt were used.

/**********/

```
#include <stdio.h>
#include <math.h>
#define infile "tvi"
#define outfile1 "standard.txt"
#define outfile2 "hamilton.txt"
#define outfile3 "simple.txt"
#define outfile4 "simple-random.txt"
double getseed(void);
void writeseed(void);
double rannos(void);
double dseed;
void main()
{
```

```
FILE *fp1, *fpout1, *fpout2, *fpout3, *fpout4;
float a, b, c;
float x[5000], x1[5000],xdata[1000], ydata[1000], y[5000], y1[5000];
float standard[1000], hstandard[1000], mcstandard[1000], rstandard[1000];
float hsumd1[1000], hsumd2[1000], sumd1[1000], sumd2[1000], mcsumd1[1000], mcsumd2[1000],
rsumd1[1000], rsumd2[100];
float hepsilon1[1000], hepsilon2[1000], hepsilon[1000],repsilon[1000], repsilon1[1000], repsilon2[1000],
mcepsilon[1000], mcepsilon1[1000], mcepsilon2[1000],epsilon1[1000], epsilon2[1000], epsilon[1000];
float pixel, rk, sk, w1, w2, w3, w4,rdatak;
int i, j, n, p, partitions, nexp, nstars;
int DD[201], DR[201], rr[201], count, RR[201];
fp1 = fopen(infile, "r");
fpout1 = fopen(outfile1, "w");
fpout2 = fopen(outfile2, "w");
fpout3 = fopen(outfile3, "w");
fpout4 = fopen(outfile4, "w");
printf("START OF PROGRAM \n");
printf("Enter the number of experiments:");
scanf("%d",&nexp);
printf("Enter the pixel partitions:");
scanf("%f", &pixel);
printf(" Enter the number of stars for the random data:");
scanf("%d", &nstars);
printf("nstars = %d \n",nstars);
partitions = (floor)((sqrt(2*2048*2048))/pixel);
printf("Partitions = %d \n",partitions);
count=0;
while(!feof(fp1))
{
count++;
```

```
fscanf(fp1, "%f %f %f", &a, &b, &c);
xdata[count] = a; ydata[count] = b;
}
for(i=1;i<=200;i++)
{
DD[i] = 0;
}
for(i=1;i<=count;i++)
{
for(j=1;j<=count;j++)
{
rdatak = sqrt((xdata[i] - xdata[j])*(xdata[i] - xdata[j]) + (ydata[i] - ydata[j])*(ydata[i] -
ydata[j]));
n = floor(rdatak/pixel) + 1;
DD[n]++;
}
}
DD[1] = DD[1] - count;
for(i=1;i<=999;i++)
{
sumd1[i] = 0;
sumd2[i] = 0;
hsumd1[i] = 0;
hsumd2[i] = 0;
mcsumd1[i] = 0;
mcsumd2[i] = 0;
rsumd1[i] = 0;
rsumd2[i] = 0;
}
getseed();
```

```
for(p=1;p<=nexp;p++)
{
for(i=1;i<=200;i++)
{
DR[i] = 0;
RR[i] = 0;
rr[i] = 0;
}
printf("Experiment #: %d \n", p);
for(i=1;i<=nstars;i++)
{
w1 = rannos();
w2 = rannos();
x[i] = 2048.0e0*w1;
y[i] = 2048.0e0*w2;
}
getseed();
for(i=1;i<=nstars;i++)
{
w3 = rannos();
w4 = rannos();
x1[i] = 2048.0e0*w3;
y1[i] = 2048.0e0*w4;
}
for(i=1;i<=nstars;i++)
{
for(j=1;j<=nstars;j++)
{
sk = sqrt((x[i] - x[j])*(x[i] - x[j]) + (y[i] - y[j])*(y[i] - y[j]));
n = floor(sk/pixel) + 1;
```

```
RR[n]++;
}
}
RR[1] = RR[1] - nstars;
for(i=1;i<=nstars;i++)
{
for(j=1;j<=nstars;j++)
{
sk = sqrt((x1[i] - x1[j])*(x1[i] - x1[j]) + (y1[i] - y1[j])*(y1[i] - y1[j]));
n = floor(sk/pixel) + 1;
rr[n]++;
}
}
rr[1] = rr[1] - nstars;
for(i=1;i<=count;i++)
{
for(j=1;j<=nstars;j++)
{
rk = sqrt((xdata[i] - x[j])*(xdata[i] - x[j]) + (ydata[i] - y[j])*(ydata[i] - y[j]));
n = floor(rk/pixel)+1;
DR[n]++;
}
}
for(i=1;i<=partitions;i++)
{
epsilon[i] = ((float)DD[i])/((float)DR[i]) - 1;
sumd1[i] = sumd1[i] + epsilon[i];
sumd2[i] = sumd2[i] + epsilon[i]*epsilon[i];
hepsilon[i] = ((float)DD[i])*((float)RR[i])/(((float)DR[i])*((float)DR[i])) - 1;
hsumd1[i] = hsumd1[i] + hepsilon[i];
```

```
hsumd2[i] = hsumd2[i] + (hepsilon[i])*(hepsilon[i]);
mcepsilon[i] = ((float)DD[i])/((float)RR[i]) - 1;
mcsumd1[i] = mcsumd1[i] + mcepsilon[i];
mcsumd2[i] = mcsumd2[i] + (mcepsilon[i])*(mcepsilon[i]);
repsilon[i] = ((float)rr[i])/((float)RR[i]) - 1;
rsumd1[i] = rsumd1[i] + repsilon[i];
rsumd2[i] = rsumd2[i] + repsilon[i]*repsilon[i];
}
}
// End of the experiments.
for(i=1;i<=partitions;i++)
{
epsilon1[i] = (sumd1[i]/(float)nexp);
epsilon2[i] = (sumd2[i]/(float)nexp);
hepsilon1[i] = (hsumd1[i]/(float)nexp);
hepsilon2[i] = (hsumd2[i]/(float)nexp);
mcepsilon1[i] = (mcsumd1[i]/(float)nexp);
mcepsilon2[i] = (mcsumd2[i]/(float)nexp);
repsilon1[i] = (rsumd1[i]/(float)nexp);
repsilon2[i] = (rsumd2[i]/(float)nexp);
}
for(i=1;i<=partitions;i++)
{
standard[i] = sqrt(epsilon2[i] -epsilon1[i]*epsilon1[i]);
fprintf(fpout1,"%d\t%f\t%f\t%d\t%d\n", i, epsilon1[i], standard[i], RR[i], DR[i]);
hstandard[i] = sqrt(hepsilon2[i] - hepsilon1[i]*hepsilon1[i]);
fprintf(fpout2,"%d\t%f\t%f\t%d\t%d\n", i, hepsilon1[i], hstandard[i], RR[i], DR[i]);
mcstandard[i] = sqrt(mcepsilon2[i] - mcepsilon1[i]*mcepsilon1[i]);
fprintf(fpout3,"%d\t%f\t%f\t%d\t%d\n", i, mcepsilon1[i], mcstandard[i], RR[i], DR[i]);
rstandard[i] = sqrt(repsilon2[i] - repsilon1[i]*repsilon1[i]);
```

```
fprintf(fpout4,"%d\t%f\t%f\t%d\t%d\n", i, repsilon[i], rstandard[i], RR[i], rr[i]);
}
fclose(fpout1);
fclose(fpout2);
fclose(fpout3);
fclose(fpout4);
writeseed();
}
//End of the main programme.
/*****************************************************************************************
double getseed(void)
{
FILE *fp;
fp = fopen("dseed.dat","r+");
rewind(fp);
fscanf(fp, "%lf", &dseed);
rewind(fp);
fclose(fp);
return dseed;
}
/*****************************************************************************/
void writeseed(void)
{
FILE *fp;
fp = fopen("dseed.dat", "r+");
rewind(fp);
fprintf(fp, "%f", dseed);
rewind(fp);
fclose(fp);
}
```

```
/*****************************************************************************
double rannos(void)
{
double d2p31 = 2147483647.0e0;
double ran;
dseed = fmod(16807*dseed,d2p31);
ran = dseed/d2p31;
return ran;
}
/*****************************************************************************/
```

Program Code C2[1]

```
/*****************************************************************************/
```

This program is designed is so that it generates a set of random co-ordinates specified by the user together with a set of gaussian distribution of points on given scale, and these gaussian points are the cluster points are the cluster points. The program works as follows will ask the user for the following input data (1)Standard deviation of distribution? Here the user must input the scale length of the cluster. (2)Total number of stars ?Here the user must input the total number of stars he wants to be on the field. (3) Fraction of stars in the cluster? Here the user must input the fraction of the total number of stars on the field he/she wants to be the cluster points (the guassian points). The results are output to the file allstars.dat.

```
/*****************************************************************************
<stdlib.h>
#include <stdio.h>
#include <math.h>
#include <limits.h>
#include "r250.h"
/* Static Variables */
static unsigned int r250_buffer[250];
static int r250_index;
```

[1]This computer code was written and designed by the advisor of this thesis and used by the author of this thesis in it's original form.

```
/* Function Protptypes */
void r250_init(int seed);
unsigned int r250();
double dr250();
/* global variables */
int seed;
double pi=3.14159265;
double xmean=1024;
double sigma;
int main()
{
int i, wi, mpoints, npoints, nstars;
double r1, r2, x1, y1, x, y, frac, rstars;
FILE *fp1, *outfile1, *outfile2;
outfile1 = fopen("allstars.dat","w+");
outfile2 = fopen("fieldstars.dat","w+");
fp1 = fopen("seedfile", "r+");
fscanf(fp1, "%d", &seed);
fclose(fp1);
r250_init(seed);
printf("Standard deviation of the distribution? ");
scanf("%lf",&sigma);
printf("Total number of stars in simulation?");
scanf("%d", &nstars);
printf("Fraction of stars in cluster?");
scanf("%lf", &frac);
rstars = frac*(double)nstars + 0.5e0;
npoints = floor(rstars);
mpoints = nstars - npoints;
printf("Number of stars in cluster: %d \n", npoints);
```

```
printf("Number of field stars: %d \n", mpoints);
for(i=1;i<=npoints;i++)
{
r1 = dr250();
r2 = dr250();
x1 = sqrt(-2.0e0*log(r1))*cos(2.0e0*pi*r2);
y1 = sqrt(-2.0e0*log(r1))*sin(2.0e0*pi*r2);
x = sigma*x1 + xmean;
y = sigma*y1 + xmean;
fprintf(outfile1, " %f %f \n",x,y);
}
/* fclose(outfile1);*/
for(i=1;i<=mpoints;i++)
{
r1 = dr250();
r2 = dr250();
x = 2048.0e0*r1;
y = 2048.0e0*r2;
fprintf(outfile1, " %f %f \n",x,y);
}
fclose(outfile1);
/* Generate an integer random number that will be used as the next seed. */
wi = r250();
fp1 = fopen("seedfile", "w+");
fprintf(fp1, "%d \n",wi);
fclose(fp1);
return 0;
}
/* r250.c the r250 uniform random number algorithm Kirkpatrick, S., and E. Stoll, 1981;
"A Very FastShift-Register Sequence Random Number Generator", Journal of Computational
Physics, V.40 also: see W.L. Maier, DDJ May 1991 */
```

```
/* set the following if you trust rand(), otherwise the minimal standard generator is used */
#define TRUST_RAND
#ifndef TRUST_RAND
#include "randlcg.h"
#endif
/* defines to allow for 16 or 32 bit integers */
#define BITS 31
#if WORD_BIT == 32
#ifndef BITS
#define BITS 32
#endif
#else
#ifndef BITS
#define BITS 16
#endif
#endif
#if BITS == 31
#define MSB 0x40000000L
#define ALL_BITS 0x7fffffffL
#define HALF_RANGE 0x20000000L
#define STEP 7
#endif
#if BITS == 32
#define MSB 0x80000000L
#define ALL_BITS 0xffffffffL
#define HALF_RANGE 0x40000000L
#define STEP 7
#endif
#if BITS == 16
#define MSB 0x8000
```

```
#define ALL_BITS 0xffff
#define HALF_RANGE 0x4000
#define STEP 11
#endif
static unsigned int r250_buffer[ 250 ];
static int r250_index;
/* Initialization function */
#ifdef NO_PROTO
void r250_init(sd)
int seed;
#else
void r250_init(int sd)
#endif
{
int j, k;
unsigned int mask, msb;
#ifdef TRUST_RAND
#if BITS == 32 || BITS == 31
srand48( sd );
#else
srand( sd );
#endif
#else
set_seed( sd );
#endif
r250_index = 0;
for (j = 0; j < 250; j++) /* fill r250 buffer with BITS-1 bit values */
#ifdef TRUST_RAND
#if BITS == 32 || BITS == 31
r250_buffer[j] = (unsigned int)lrand48();
```

```
#else
r250_buffer[j] = rand();
#endif
#else
r250_buffer[j] = randlcg();
#endif
for (j = 0; j < 250; j++)/* set some MSBs to 1 */
#ifdef TRUST_RAND
if ( rand() > HALF_RANGE )
r250_buffer[j] |= MSB;
#else
if ( randlcg() > HALF_RANGE )
r250_buffer[j] |= MSB;
#endif
msb = MSB; /* turn on diagonal bit */
mask = ALL_BITS; /* turn off the leftmost bits */
for (j = 0; j < BITS; j++)
{
k = STEP * j + 3; /* select a word to operate on */
r250_buffer[k] &= mask; /* turn off bits left of the diagonal */
r250_buffer[k] |= msb; /* turn on the diagonal bit */
mask >>= 1;
msb >>= 1;
}
}
/* Function to generate random unsigned integer */
unsigned int r250() /* returns a random unsigned integer */
{
register int j;
register unsigned int new_rand;
```

```
if ( r250_index >= 147 )
j = r250_index - 147; /* wrap pointer around */
else
j = r250_index + 103;
new_rand = r250_buffer[ r250_index ] ^ r250_buffer[ j ];
r250_buffer[ r250_index ] = new_rand;
if ( r250_index >= 249 ) /* increment pointer for next time */
r250_index = 0;
else
r250_index++;
return new_rand;
}
/* Funtion to generate random double in the range 0 .. 1 */
double dr250() /* returns a random double in range 0..1 */
{
register int j;
register unsigned int new_rand;
if ( r250_index >= 147 )
j = r250_index - 147; /* wrap pointer around */
else
j = r250_index + 103;
new_rand = r250_buffer[ r250_index ] ^ r250_buffer[ j ];
r250_buffer[ r250_index ] = new_rand;
if ( r250_index >= 249 ) /* increment pointer for next time */
r250_index = 0;
else
r250_index++;
return (double)new_rand / ALL_BITS;
}
```

Program Code C3

```
/*this program is designed to solve the cubic equation 4.10.*/

#include <stdio.h>

#include <math.h>

#define infile "UBVRI"

#define outfile "deredding.txt"

#define outfile1 "color-excess.txt"

void main()

{

FILE *fp, *fp1, *fp2;

float a, b, c, d, e, f, g, m, x1,ds[1000], Eub[1000], Ebv[1000], Av[1000], x2;

float a2, a3, a4, a5, a6, a7, a8, a9, a10, a11, a12, a13;

float x[1000], y[1000], q[40];

float xc[40], yc[40], v[40], dv[40], bv[40], dbv[40], ub[40], dub[40], vi[40], dvi[40], vr[40], dvr[40];

int i, j, maxit, a1, star[40];

fp = fopen( infile, "r");

fp1 = fopen(outfile, "a");

fp2 = fopen(outfile1, "a");

a = +8.93830; b = -27.5360; c = +23.5150; d = +0.00000; e = -7.65860; f = +1.98420; g =
-0.02578; m = +0.72000;

i = 0;

while(!feof(fp))

{

i++;

fscanf(fp," %d %f %f %f %f %f %f %f %f %f %f %f %f ", &a1, &a2, &a3, &a4, &a5, &a6,
&a7, &a8, &a9, &a10, &a11, &a12, &a13);

star[i] = a1 ; xc[i] = a2 ; yc[i] = a3; v[i] = a4 ; dv[i] = a5; ub[i] = a6 ; dub[i] = a7; bv[i] = a8;
dbv[i = a9 ; vr[i]= a10 ; dvr[i] = a11 ; vi[i] = a12 ; dvi[i] = a13 ;

}

for(j=1;j<=30;j++)
```

```
{
q[j] = (ub[j]) - 0.72*(bv[j]);
}
printf("Enter the value x1, x2 and max number of iteration :");
scanf(" %f %f %d", &x1, &x2, &maxit);
for(i=1;i<=30;i++)
{
for(j=2;j<=maxit;j++)
{
x[1] = 0.5*(x1 + x2);
x[j] = x[j-1] - (a*pow(x[j-1],6) + b*pow(x[j-1],5) + c*pow(x[j-1],4) + d*pow(x[j-1],3) + e*pow(x[j-1],2) + (f-m)*(x[j-1]) + g - q[i])/(6*a*pow(x[j-1],5) + 5*b*pow(x[j-1],4) + 4*c*pow(x[j-1],3) + 3*d*pow(x[j-1],2) + 2*e*(x[j-1]) + f - m);
y[j] = 0.72*x[j] + q[i];
Ebv[j] = bv[i] - x[j];
Eub[j] = ub[i] - y[j];
Av[j]= 3*Ebv[j];
ds[j]= Av[j]/0.0015;
}
fprintf(fp2,"%d\t%f\t%f\n", star[i], Ebv[maxit], Eub[maxit]);
}
fclose(fp);
fclose(fp1);
fclose(fp2);
}
```

Program Code C4

```
/* This program is designed to calculate the auto-corelation function. */
#include <stdio.h>
#include <math.h>
```

```
#define infile "tvi"
#define outfile1 "stardensity-two-point.txt"
int sum[16], countk[15], cell[19][19];
float N[15][15];
void main()
{
FILE *fp, *fpout1;
float epsilon[16], epsilon0[16],epsilon1[16];
float coords[350][2], mean, x, y, z;
float ratio, a, b, variance, standev, sum, sum2;
int i, j, k;
int count, maxcount;
fp = fopen( infile, "r" );
fpout1 = fopen( outfile1, "w" );
count=0;
maxcount = 0;
while (!feof(fp) ) /* reads data (star co-ordinates) from infile into a 1-D array coords*/
{
count++;
fscanf(fp, "%f %f %f", &x, &y, &z);
coords[count][1] = x; coords[count][2] = y;
i = floor(x/128.0e0) + 1; // The stars are put into cells
if(x == 2048) i = 16;
j = floor(y/128.0e0) + 1;
if(y == 2048) j = 16;
cell[i][j] = cell[i][j]++;
maxcount++;
//printf("%d\n", maxcount);
}
for(j=16;j>=1;j--)
```

```
{
for(i=1;i<=16;i++)
{
N[i][j] = 0;
// cell[i][j] =0;
}
}
for(i=1;i<=16; i++)
{
for(j=1;j<=16; j++)
{
sum = sum + cell[i][j];
mean = sum/(16*16);
sum2 = sum2 + (mean - cell[i][j])*(mean - cell[i][j]);
}
}
variance = sum2/299;
standev = sqrt(variance);
printf(" The standard deviation is  %f \n", standev);
printf(" The mean number of stars per cell is = %f \n", mean);
printf("\n");
for(j=16;j>=1;j–)
{
for(i=1;i<=16;i++)
{
printf(" %d ", cell[i][j]);
}
printf("\n");
}
for(k=1;k<=15;k++)
```

```
{
for(i=1;i<=16;i++)
{
for(j=1;j<=16-k;j++)
{
epsilon0[k] = epsilon0[k] + ((float)cell[i][j])*((float)cell[i][j+k]);
countk[k]++;
}
}
}
for(k=1;k<=15;k++)
{
for(j=1;j<=16;j++)
{
for(i=1;i<=16-k;i++)
{
epsilon1[k] = epsilon1[k] + ((float)cell[i][j])*((float)cell[i+k][j]);
}
}
}
for(k=1;k<=15;k++)
{
epsilon[k] = (epsilon0[k] + epsilon1[k])/(((float)countk[k])*2);
epsilon[k] = epsilon[k]/(mean*mean) - 1;
}
printf("\n");
for((k=1);(k<=15);k++)
{
fprintf(fpout1," %d\t%f\n", k, epsilon[k]);
}
```

```
printf("\n");
printf(" Goto stardensity-two-point.txt for results of the two point corelation function.\n");
printf("\n");
for(j=16;j>=1;j–)
{
for(i=1;i<=16;i++)
{
a = ((cell[i][j] - mean)*(cell[i][j] -mean)/256);
N[i][j] = ((cell[i][j])*(cell[i][j])/(mean) - 1);
}
}
for(j=16;j>=1;j–)
{
for(i =1;i <=16; i++)
{
printf(" %4.2f ", N[i][j]);
}
printf("\n");
}
ratio = sqrt(a/mean);
b = sqrt(mean);
printf(" ratio = %f root of mean = %f m-observations = %f \n ", ratio, b, a);
}
```

Bibliography

[1] Ballantyne, D.R. *et al.*, 2000, ApJ, **539**, 283.

[2] Belikov, A.N. *et al.*, 2000, A&A, **358**, 886.

[3] Bessell, M. S., 1990, Publication of the Astronomical Society of the Pacific, **102**, 1811-1199.

[4] Bradley, W. C. & Dale, A. O., 1996, *Modern Astrophysics*, Addison-Wesley Publishing Company, 437-474.

[5] Bonnel, I. A. & Davies, M.B., 1998, MNRAS, **295**, 691

[6] Bowers, R. & Deeming, T., 1984, *Astrophysics 1: Stars*, Jones and Bartlett Publishers Inc, 35.

[7] Brown, A. G. A., *et al.*, 1991, eds: Lada, C. J. & Kylafis, D. N., *The Origins of Stars and Planetary Systems*, Kluwer Academic Publishers, 419.

[8] Cabrit, S., 1992, *Star Formation and Techniques in Infrared and Millimeter Wave Astronomy*, lectures held at the Predoctoral Astrophysics School V, Springer-Verlag.

[9] Churchwell, E. D., 1991, eds: Lada, C. J & Kylafis, N. D., *The Physics of star Formation and Early Stellar Evolution*, Kluwer Academic Publishers, 221-22.

[10] Elmegreen, B. G., 1987, Interstellar Processes, eds: Hollenbach, D. J. & Thronson, H.A., Reidel Publishing Co., 259-280.

[11] Gilliland, R. L., 1992, eds: Howell, S. R., *Astronomical CCD Observing and Reduction Techniques*, ASP Conference Series, **23**, 77-78

[12] Gullixson, A. C., 1992, eds: Howell, S. R., *Astronomical CCD Observing and Reduction Techniques, ASP Conference Series*, **23**, 130-157.

[13] Goedhart, S., van der Walt, D. J. and Gaylard, M. J., 2001, MNRAS, 1-6.

[14] Garmany, C. D., *Astronomical Society of the Pacific*, 1994, **106**, 2.

[15] Herbig, G. H., 1998, ApJ, **498**, 736-557.

[16] Hermit S., *et al.*, 1996, MNRAS, **283**, 709.

[17] Heydari-Malayeri, M., 1988, *Astron. Astrophys,* **202,** 240-252.

[18] Hillenbrand, L. A., *et al.*, 1993, ApJ, **106**, 1906.

[19] Lada, C. J., 1999, eds: Lada C. J. & Kylafis, N. D., *The Origins of Stars and Planetary Systems*, Kluwer Academic Publishers, 143.

[20] Lada, C. J., 1991, eds: Lada, C. J. & Kylafis, N. D., *The Physics of star Formation and Early Stellar Evolution*, Kluwer Academic Publishers, 329-330.

[21] Lee, J. K., Walsh A. J., Burton, G. M., Ashley B. C., 2000, MNRAS, 1-7.

[22] Lang, K. R., 1999., *Astrophysical Formulae: Space, Time, Matter and Cosmology*, Springer-Verlag, **2**, 282

[23] Pandey, A. K. *et al.*, 2001, A&A, **374**, 504-522.

[24] Peebles P. J. E., 1980, *The Large-Scale Structure of the Universe*, Pinceton University Press, New Jersey.

[25] Scheffler, H. & Elsasser, H., 1988, *The Physics of the Galaxy and Interstellar Matter,* Spring-Verlag Berlin Heidelberg, 56, 156.

[26] Seab, C. G., 1995, *Astronomy*, Springhouse Co., 118-122.

[27] Mazurek, T. J., 1980, A&A, **90**, 65.

[28] Nekel & Klare, 1980,

[29] van den Ancker, M., E. *et al,* 1996,

[30] Vittone, A. A., de Martino, D., Ginovanelli, F. and Rossi, C., 1987, *Astron. Astrophys.* **179**, 157-163.

[31] Vrba, F., J., *et al.*, 2000, ApJ, **533**, 17-20.

[32] Walsh, A. J., Bertoldi, F., Burton, M. G., Nikola, T., 2001, MNRAS, **326**, 36 .

[33] Whitworth, A., 1979, MNRAS, **186**, 59.

[34] Wouterloot, J. G. A., Brand, J., 1989, A&A, **80**, 149.

[35] Zeilik, M. & Gregory, S. A., 1998, *Astrophysics & Astronomy, fourth edition*, John Vondeling Publishers, 230-232.